Volume 3 *August, 1932* *Number 2*

PHYSICS

The X-Ray Method of Determining the Sizes of Sub-Microscopic Crystals*

By G. HARVEY CAMERON
E. I. duPont de Nemours and Company, Wilmington, Delaware

(Received June 16, 1932)

A brief critical summary of the principal contributions published on the theory of the subject is presented, followed by the report of a series of experiments designed to test the methods which have been proposed. It is concluded that while relative measurements can be made with sufficient accuracy, absolute values cannot be relied on as yet. The results emphasize the necessity for careful attention to such details as the construction of the camera, the preparation of the sample, and the characteristics of the x-ray film and of the microphotometer.

I. INTRODUCTION

THE x-ray method of determining particle-sizes depends on the fact that sub-microscopic crystals give rise to broad diffraction lines in the powder diagram. The apparatus used consists of a source of monochromatic x-rays, a slit-system to define the x-ray beam, and a cylindrical camera on the axis of which the sample to be studied is mounted. If the crystals composing the sample are small enough, the diffraction lines are broadened in excess of the value determined by the dimensions of the x-ray beam and of the sample. It is the purpose of this paper (1) to review the attempts which have been made to derive relationships between the particle-sizes and the breadths of the diffraction lines, since most of this work has been published abroad and may not be readily accessible, and (2) to give the results of our work on the application of these methods to particular cases. This work was undertaken not only to obtain answers to specific problems but also to find out as much as possible about the methods which have been proposed, their range of applicability, their accuracy, and the most suitable techniques. The work is admittedly incomplete and several difficulties have remained unsolved, but it is believed that our experiences will be of value to others who are contemplating the use of these methods.

II. SUMMARY OF THE THEORETICAL BACKGROUND

In 1918, Scherrer[1] published the following equation relating line-breadth to particle-size:[2]

$$B = 2(\ln 2/\pi)^{1/2}(\lambda/\Lambda)(1/\cos\theta/2) + b \qquad (1)$$

* Communication No. 103 from the Experimental Station of E. I. duPont de Nemours and Company.

[1] Scherrer, in Zsigmondy, Kolloidchemie 3rd Ed. pp. 387–409.

[2] The exact meaning of the term *particle-size* is given on page 59 in the explanation of von Laue's formulas.

B is the line-breadth divided by R, the radius of the camera, λ is the wavelength of the x-radiation, Λ is the particle-size, θ is the angle between the incident and the diffracted beams, and b is a constant depending on the dimensions of the apparatus. The line-breadth is defined, in the derivation of all particle-size formulas, as the ratio of the integral of the intensity across the diffraction line to the maximum intensity. This measurement would be difficult to make in practice and the quantity actually measured is the distance between the two points on the line where the intensity is half the maximum. The two definitions are, of course, equivalent only for diffraction lines of special shapes.

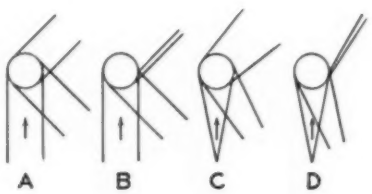

Fig. 1. *A*, parallel radiation, transparent sample; *B*. parallel radiation, opaque sample; *C*, divergent radiation, transparent sample; *D*, divergent radiation, opaque sample.

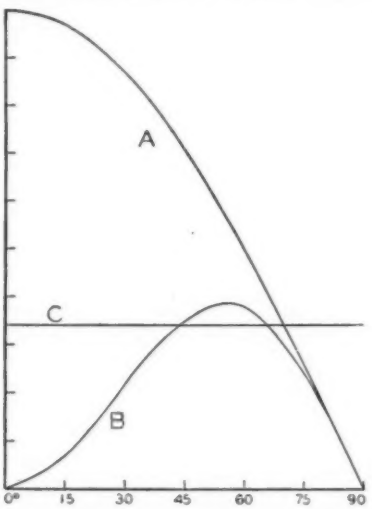

Fig. 2. Line-breadth for infinitely large particles (after Brill). Abscissas: The half diffraction angle $\theta/2$ in degrees. Ordinates: Relative line-breadth. *A*, divergent radiation, transparent sample; *B*, divergent radiation, opaque sample; *C*, parallel radiation, transparent sample.

This equation was derived with the aid of the following assumptions: (1) that the crystal lattice of the sample is cubic, (2) that the particles are oriented at random, (3) that the absorption of x-rays in the sample can be neglected, (4) that the particles are similar in shape and equal in size, (5) that the lattice is undistorted, and (6) that the incident radiation is parallel. In practice the breadths, B, are plotted against $1/(\cos\theta/2)$; the slope of the resulting straight line is proportional to $1/\Lambda$, while the intercept on the B axis is equal to b.

In addition to the limitation to crystals of the cubic system, the use of Scherrer's formula has the serious drawback that parallel radiation and a totally transparent sample cannot be realized. Moreover, the best approximations to these conditions which are experimentally feasible still leave much to be desired, as has been determined by Brill[3] and others. Scherrer expressed the breadth B of a diffraction line as the sum of two terms, the first a function of the angle θ and the size of the particles, the second a constant depending only on the dimensions of the sample and the slit system. For "infinitely" large particles the first term becomes zero and B is independent of θ. Now if the radiation is *not* parallel, the breadths[4] of the lines will decrease with θ; if the sample is *not* transparent the breadths will tend to increase with θ. See Figs. 1 and 2. Hence, these two defects will oppose each other and in favorable cases the Scherrer condition may accidentally be realized. This appears to be the explanation of the excellent results obtained with the Scherrer equation in some cases, for example, Scherrer's own determinations of the particle-size of colloidal gold.[1]

In 1926, von Laue[5] derived a formula which has been used as the basis for most of the subsequent work. His assumptions were the same as Scherrer's except that the lattice-structure of the crystals need not be cubic and that the radiation was assumed to be purely divergent. The expression is as follows:

$$B = \frac{\pi \frac{\omega}{\eta}\left(\frac{r}{R}\right)^2 \cos^3\frac{\theta}{2}}{1 + \left(\frac{\omega r}{\eta R}\,\frac{\cos^2\frac{\theta}{2}}{2}\right)^2 - 1}$$

which when solved for η becomes:

$$\eta = (\omega/2\pi)(B\cos\theta/2 - (1/B)(\pi r/R)^2\cos^3\theta/2) \tag{2}$$

where $\omega = \text{const.} = 0.55$, r is the radius of the sample, R, the radius of the camera, and η is a quantity related to the particle-size by the following equation:

$$\eta(h_1, h_2, h_3) = \frac{\lambda}{4\pi}\left[\sum\left(\frac{\mathfrak{b}_i\mathfrak{H}}{m_i}\right)^2\right]^{1/2} \tag{3}$$

where

$$\mathfrak{H} = \sum h_i\mathfrak{b}_i/\left|\sum h_i\mathfrak{b}_i\right| \quad \text{and} \quad b_i = [\mathfrak{a}_k\mathfrak{a}_l \quad a_1a_2a_3$$

Here λ is again the wave-length, h_i are the Miller indices of the crystal planes concerned, $\mathfrak{b}_i$ are the unit vectors of the reciprocal lattice, and m_i are the numbers of unit lengths in the directions of the unit vectors $\mathfrak{a}_i$ of the elementary parallelopiped. The notation is that of von Laue except that

[3] Brill, Zeits. f. Krist. **68,** 387 (1928).

[4] For purely divergent radiation and infinitely large particles the line-breadths $B = (\pi r/R)\cos\theta/2$, according to Eq. (2), page 59.

[5] von Laue, Zeits. f. Krist. **64,** 115 (1926).

he used χ instead of θ. Moreover, his B had a different meaning.[6] For the cubic system Eq. (3) reduces to

$$\eta = \lambda/(4\pi am) = \lambda/(4\pi\Lambda) \tag{4}$$

where Λ is again the particle-dimension.

A condition which gives the limits within which the departure from purely divergent radiation can be neglected was also derived by von Laue as follows:

$$5/8\omega^2 \cos\theta/2(T/\eta)^2 \gtrsim 1. \tag{5}$$

T is the *Oeffnungswinkel*, i.e., the pinhole diameter divided by the radius of the camera.

So far all the theories had assumed that the sample consisted of particles of uniform size, obviously a fiction introduced for mathematical convenience. Patterson[7] took over von Laue's method and added the assumption that the sizes of the particles are distributed numerically according to the Maxwell law, $N_{(\mu)} = \mu^2 e^{-p^2\mu^2}$ where μ is a quantity proportional to the particle-size and $N_{(\mu)}$ is the number of particles having the size corresponding to μ. Patterson's calculation leads to the result that, if von Laue's formula for the calculation of η is blindly applied to a material the particles of which are distributed according to the Maxwell law, the value obtained will be approximately equal to $\bar{\eta}/\pi^{\frac{1}{2}}$ where $\bar{\eta}$ is the mean of the values of η for the individual particles. The true mean particle-size cannot therefore be deduced without an exact knowledge of the distribution. Mark[8] objected to the assumption of a Maxwell law as favoring the large particles at the expense of the small ones and stated that a distribution law of the Gauss *error* type $N_{(\mu)} = e^{-(\mu-\mu_0)^2 p}$ would seem a more reasonable choice. Without giving the details of the calculation he added that if a material has the Gauss distribution, the result obtained by direct application of von Laue's formula will be only slightly in error.

Brill,[3] and Brill and Pelzer[9,10] contributed three modifications of von Laue's theory. These have the advantage that the assumptions more closely approximate actual experimental conditions.

The first dealt with specimens which absorbed the x-rays appreciably. Assuming a solid cylindrical sample in which there was complete absorption, Brill showed that for infinitely large particles the experimental line-breadths, B', would be connected with the B used by von Laue by the equation

$$B = B'/\sin^2(\theta/2). \tag{6}$$

[6] In von Laue's Eq. (46), which has been quoted by several authors, the quantity B is expressed in a different scale and must be multiplied by $2/(\cos\theta/2)$ before it can be applied to experimental work.

[7] Patterson, Zeits. f. Krist. **66,** 637 (1928).

[8] Mark, Trans. Far. Soc. **25** 387 (1929).

[9] Brill and Pelzer, Zeits. f. Krist. **72,** 398 (1929).

[10] Brill and Pelzer, Zeits. f. Krist. **74,** 147 (1930).

His procedure was to correct the measured line-breadths by Eq. (6) and then to calculate particle-sizes by means of Eqs. (2) and (3). Finally since in any particular case absorption may not be complete in a thin layer at the surface, the calculated particle-sizes were plotted against $\sin^2 \theta/2$ and extrapolated to find the particle-size for $\sin^2 \theta/2 = 1$ since at $\theta = 180°$ absorption presumably has no effect.

This treatment imposes two limitations upon the general application of the method. The accuracy of the final result obviously depends upon having one or more diffraction lines at large angles, which is often difficult to achieve. In the second place, it is not possible to get any information about the shape of the particles since the treatment tacitly assumes that all dimensions are equal.

In addition to these limitations, it is perhaps worthwhile to point out some inconsistencies which may be sources of significant error. The correction for absorption embodied in Eq. (6) was developed for *sharp* lines, i.e., nothing was said about the effect of absorption on the broadening due to particle-size in the derivation of this equation. Moreover, it was developed for parallel radiation while the von Laue theory was based on the use of purely divergent rays. The experimental work presented later will show that many of the

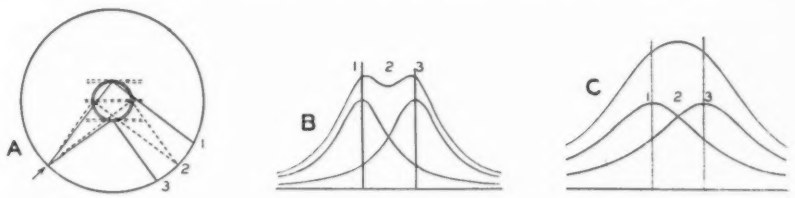

Fig. 3. The hollow-sample method (after Brill). *A*, horizontal section through camera and sample (size of sample much exaggerated); *B*, double peak; *C*, single peak formed by very small particles.

published results must be discounted for lack of attention to the definition of the incident x-ray beam.

The second method[9] employed the sample in the form of a thin-walled hollow cylinder. The slit system had a single pinhole-opening on the circumference of the camera, which was placed as close as possible to the target of the tube so as to give divergent radiation. The rays encountered a greater thickness of material at the sides of the sample than in going through the tube and consequently the diffraction lines appeared double. See Fig. 3. The authors adapted von Laue's theory to this arrangement and published a curve relating the separation of the peaks to the particle-size of the sample. When the particle-size is quite small the two peaks may fuse into one. The authors showed that the particle-size may be determined from a measurement of the line-breadth with the aid of a formula developed for this special case. The theory of this method is free from the inconsistencies of the first method; furthermore, it enables size-determinations to be made from a single diffraction line, and hence the shape of the particles may be investigated.

The third method[10] is closely related to the second. The arrangement of the camera was the same, but the sample was made quite opaque. Materials whose absorption was not sufficient to accomplish this were coated thinly on a lead glass rod of suitable diameter. The theory postulates that only crystals in a thin layer of the material struck by the direct rays from the pinhole shall be effective in producing the diffraction lines. See Fig. 4. This means that in deriving the expression for the diffracted energy in a given line of the pattern, the integration is to be made over the arc *BCD* instead of completely around the circumference as in the method above. Unfortunately the authors integrated over 180 degrees, i.e., the arc *ACE*, apparently to avoid a difficult mathematical problem. This amounts again to assuming parallel radiation in part of the theory. In Part III evidence will be presented to show that this inconsistency may be significant. The particle-size is to be calculated from a family of curves published by the authors. See Fig. 7. Values of b/r (the linear line-breadth divided by the radius of the sample) are plotted against θ and the corresponding values of η obtained by interpolation. This method, like the preceding one, enables a particle-size determination to be made from a single diffraction line and hence offers the possibility of investigating the shape of the crystals. In a later article[11] Brill has studied this phase in more detail.

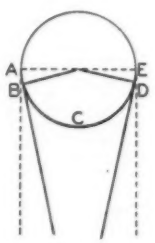

Fig. 4.

III. Experimental Details

The x-rays were produced by a Siegbahn-Hadding tube with interchangeable targets excited at approximately 46 k.v. and carrying 13 to 15 m.a. Copper and iron targets were used with their appropriate filters. Agfa x-ray film was used in all the work reported. Particular pains were taken to have the photographic conditions uniform. The films were developed for five minutes at 18°C using the elon-hydroquinone developer recommended for this emulsion; the trays were hand-rocked to ensure uniform development.

Test of exposure-density relation and of microphotometer characteristics

For the interpretation of the diffraction photographs it is almost essential that there be a linear relationship between the intensity of the x-rays producing a given deposit on the film and the deflection of the galvanometer when the spot is photometered, since any method of correcting for the want of linearity would be extremely tedious. To study this relationship, exposures were made on the type of film to be used in the subsequent work, the films

[11] Brill, Zeits. f. Krist. **75**, 217 (1930).

being held in a cassette 2 meters from the x-ray tube. On each film five or six exposures were made varied in suitable steps. Seven sets made when the tube was operating most satisfactorily were used to plot the curve shown in Fig. 5. This procedure is only valid if time of exposure and intensity of radiation are strictly equivalent, i.e., γ must be unity in the equation, $It^{\gamma}=1$, the so-called *reciprocity* relation. Bouwers[12] has shown that for x-rays $\gamma=1$ to within one percent, so that the method is no doubt justified.

Fig. 5 shows the relationship observed between relative exposures and deflections produced in the galvanometer. The curve closely approximates a straight line for low densities, and tests have shown that no appreciable error is introduced provided deflections greater than 35 mm, corresponding to densities[13] greater than about 0.7, are avoided. The latter figure was obtained by photometering a calibrated neutral wedge since density determinations with the microphotometer alone were in error by as much as 50 percent due to the character of the illumination.

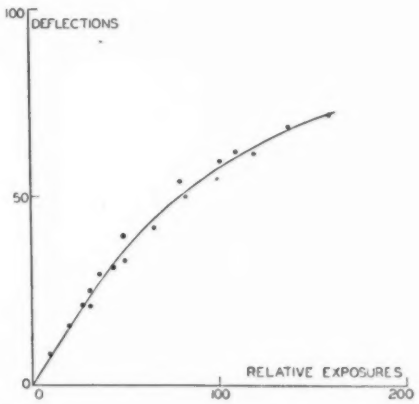

Fig. 5. Test of x-ray film and photometer characteristics. Abscissas: Relative exposures to x-rays. Ordinates: Deflections of galvanometer in mm.

Tests of the Scherrer and von Laue methods with colloidal gold

In order to get information as to the accuracy of these methods both as to relative and absolute values of particle-size and also as to the effect of the distribution of sizes in the sample, experiments were undertaken with colloidal gold solutions of which the mean size and size-distribution could be determined by an independent method.

A series of five sols was prepared following closely the method of Rinde.[14] The nuclear sol was prepared by reducing chlorauric acid with phosphorus from water solution; sols of larger particle-size, by reducing with 33 percent hydrogen peroxide in the presence of a definite amount of the nuclear sol.

[12] Bouwers, Zeits. f. Physik **14,** 374 (1923).

[13] Density is defined as $D=\log_{10} i_0/i$ where i_0 is the intensity of the incident light and i, that of the transmitted. In photographic sensitometry the measurement is ordinarily made in diffuse light, which is not possible in the ordinary microphotometer.

[14] Rinde, Dissertation, Upsala, 1928. In English.

By thus using each sol as a nuclear sol for the next larger, gold particles having any required size could be built up. The well-known precautions as to purity of ingredients and cleanliness of vessels were strictly adhered to. The sols were stabilized with gelatine, dialyzed with redistilled water for 24 hours or more to remove salts, and finally evaporated to dryness. Control experiments were performed to ensure that no step in this treatment altered the character of the sol. In each case a sample of the original sol was reserved for study in the ultra-centrifuge.

The evaporated gold, which was somewhat plastic due to the gelatine, was formed into a cylindrical rod by packing it into a tiny glass tube and then extruding it about 3 mm from one end. The glass tube was then mounted on the axis of the camera.

The camera used for these tests had a radius of 49.4 mm; the slit system was the conventional Debye-Scherrer arrangement with pinholes 1 mm in diameter. The diameters of the samples ranged between 0.4 and 0.7 mm.

TABLE I. *Particle-sizes of gold sols in angstroms.*

	C_1	C_2	C_3	C_4	C_5
Scherrer equation			47	62	81
Laue equation	32	38.5	52	65	87
Brill method Cu radiation			47	58	82
Fe radiation	30.5	42			
Ultra-centrifuge	40	61	100	149	225

Table I shows the results obtained with these sols. The first line gives sizes for three sols derived by means of the Scherrer equation, the values being found by the use of least squares. The second line gives results obtained by directly applying the von Laue equation which assumes no absorption in the sample. The next set of figures were found by the Brill method which allows for absorption in the sample but is otherwise identical with the preceding. In the last line are figures derived from the published measurements on these sols by Rinde. These values were in good agreement with measurements made in this laboratory by Dr. J. B. Nichols.[15] Strictly speaking, the ultra-centrifuge determines the particle-size distribution on a weight basis, i.e., the distribution curve represents relative total weights of particles in the sample having a given diameter. The values given in Table I have been transformed to a number basis and represent the size of the most frequently occurring particles which is very close to the average size since the distribution is nearly symmetrical. These values are of course not very accurate, but in view of the large discrepancy between them and the x-ray data this is unimportant.

The source of this discrepancy is not obvious. The ultra-centrifuge method has received more intensive study than the x-ray, and has yielded particle-size determinations on gold sols and other materials in satisfactory agreement with those obtained by independent methods such as osmotic pressure

[15] For a brief description of the ultra-centrifuge and the method of particle-size determination, see Nichols, Physics **1**, 254 (1931).

and the ultra-microscope. At first sight, one would therefore be inclined to give greater weight to the values obtained by its use. On the other hand, the x-ray method is the only one which distinguishes between a single crystal and a crystalline aggregate. The fact that the disagreement in the results is relatively much worse in the sols of larger particle-size is perhaps evidence that there is some aggregation taking place. However, later work has shown how important is the geometrical definition of the x-ray beam, and consequently too great reliance cannot be placed on the x-ray results in Table I on account of the failure to provide either strictly parallel or purely divergent radiation. The agreement of the values obtained by the Scherrer formula with the other x-ray data must be partly fortuitous[16] due to a favorable balance between absorption and divergent radiation as indicated on page 59.

Additional conclusions which may be drawn from this work are, first, that, although the absolute values may be seriously in error, any of the three

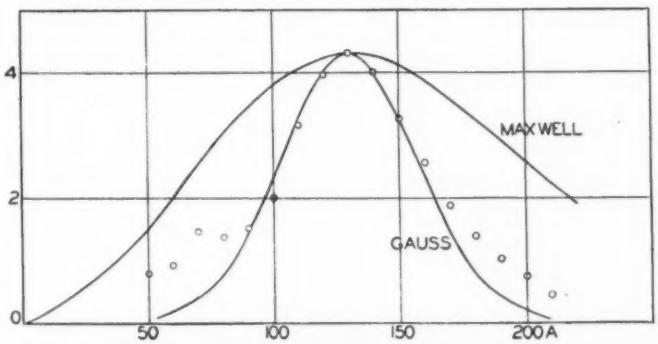

Fig. 6. Size distribution of a colloidal gold solution. Abscissas: Particle-radius in angstroms. Ordinates: Relative number of particles. Note: The values for small particles are too high on account of a systematic error introduced by the microphotometer which has since been eliminated.

methods used is capable of arranging the series in the correct order of size with considerable precision. In the second place the particle-size distribution curves as obtained by Dr. Nichols for these sols, when placed on a number basis approximate quite closely the error type of curve and not at all, the Maxwell law. Fig. 6 shows this result for one sol. According to Mark, therefore, the effect of the distribution of sizes on the value obtained by x-rays will be small.

It might also be mentioned that this work furnishes direct proof—for the first time, it is believed—that a colloidal particle formed by the nuclear method does grow by extending the crystal lattice, as indeed has long been supposed.

Tests of the Brill and Pelzer hollow-sample method

The results reported in the preceding section indicated that insufficient care had been taken by the writer and by others in defining the character of

[16] In some preliminary experiments using samples of lower atomic weight, negative values of particle-size were obtained. The explanation for this is suggested by Fig. 2.

the x-ray beam. Accordingly a camera was built to give as nearly purely divergent radiation as possible. An examination of Eq. (5), above, shows that with cameras of reasonable dimensions only samples having extremely small particle-size will satisfy von Laue's condition. For example, given a camera of 10 cm diameter with a pinhole 0.25 mm in diameter the largest particle-size which will satisfy Eq. (5) is about 60A.

On account of the great difficulty of allowing mathematically for the finite size of the pinhole, the device of varying its size experimentally was resorted to. Three pinholes were constructed having diameters of 0.66, 0.46 and 0.24 mm and arranged so as to lie accurately on the circumference of the camera. A sample of magnesium oxide was prepared by casting a thin film from a suspension in collodion, wrapping it around a copper wire and slipping the wire, which had been very lightly greased, out of the tube. Diffraction photographs were then made with each of the pinholes without disturbing the sample. The films showed clear-cut double lines which gave excellent photometer records. The particle-size values, which are tabulated in Table II, are seen to vary considerably with the size of the pinhole. Brill and Pelzer[9] also used this method to determine the particle-diameter of magnesium oxide and reported the values given in the last column of the table. They did not give the dimensions of the apparatus used.

TABLE II. *Particle-size of magnesium oxide in angstroms.*

Indices	Pinhole 0.66 mm	0.46 mm	0.24 mm	0 mm extrapolated	Brill & Pelzer
100	52	59	65	72	49
110	57	61	81	88	57
111	.	80	95	106	54

Attempts were made to apply the hollow-sample technique to titanium dioxide, colloidal silver and two different preparations of colloidal gold but without obtaining any satisfactory diffraction patterns. Titanium dioxide alone gave one line which showed a suggestion of the double peak. It was concluded that these materials are too absorbing even in such thin tubes and that the method can only be applied successfully to very transparent substances.

Tests of the "total absorption" method with colloidal platinum

Four platinum black catalysts made by different procedures[17] were used to test this method. The samples were prepared by very lightly greasing a lead glass rod of appropriate diameter, dusting it with the colloidal metal and finally rolling the preparation on a glass plate. The photographs were made in the camera previously described, all three pinholes being used in most cases. Exposures of from 8 to 26 hours were required depending on the size of the pinhole. At least four diffraction lines were measurable in all cases. The results are displayed in Fig. 7.

[17] Taylor, Kistiakowsky and Perry, J. Phys. Chem. **34,** 748 (1930).

In the case of Pt. Black No. 1, curves for the largest and smallest pinholes are plotted. There was again a strong dependence of the apparent particle-size on the diameter of the pinhole, as the curves and Table III show.The points fitted the theoretical curves well with the exception of the measurements for the first two diffraction lines, which, in every case, fell above the curves. The only reasonable explanation of this which can be suggested is that the layer giving rise to the diffraction lines at small angles was not sufficiently thin or opaque and hence gave lines of excessive breadth.

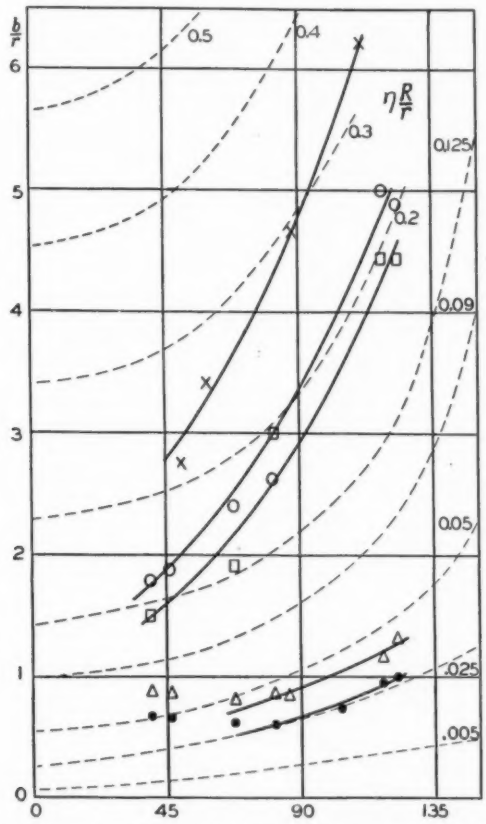

Fig. 7. Particle-size determination by the *total absorption* method. Dotted lines are theoretical curves. Solid lines are experimental: Crosses—Pt. Black No. 4, Large Circles—Pt. Black No. 3, Squares—Pt. Black No. 2, Triangles—Pt. Black No. 1, largest pinhole, Small Circles—Pt. Black No. 1, smallest pinhole. Abscissas: Diffraction angle θ.

TABLE III. *Pt. Black No. 1.*

Pinhole diameter	Particle-size
0.66 mm	290A
0.46	313
0.24	430
0 extrapolated	over 500

Pt. Blacks Nos. 2 and 3 gave very diffuse diffraction lines indicating that they were much more finely divided than No. 1. When the data were plotted it was observed that they no longer fitted Brill's curves, the lines being much too narrow at small angles. In order to vary the experimental conditions, a new platinum preparation was made and photographed with iron radiation; the previous results were all obtained with copper. The resulting curve, designated as Pt. Black No. 4, is consistent with those for Nos. 2 and 3.

The results suggest that the theory may be in error because of the inconsistency referred to on page 62 and in Fig. 4. Although the inaccuracy in placing the limits of integration would have little effect on the breadths of the lines at large angles, it might be quite important at small angles and would act in the direction required by the curves presented, i.e., the theoretical breadths at small angles would be less.

If the line-breadths at large angles are taken as more probably correct, the particle-sizes obtained with the smallest pinhole are, for Pt. Blacks Nos. 2 and 3, about 60A; for Pt. Black No. 4, about 50A.

Experiments with mixtures

In order to obtain some idea experimentally of the effect of the distribution of sizes it had been planned to make up samples having various artificial size-distributions which could be determined with the ultra-centrifuge and hence correlated with the x-ray findings. It was not possible to carry out this program; however two preliminary experiments will be reported for what they are worth. Two mixtures of Pt. Blacks Nos. 1 and 3 were prepared and particle-size determinations made by the total absorption method using the smallest pinhole. The results were as follows.

Percent of Pt. Blk. No. 1 in mixture	Apparent particle-size with smallest pinhole
0%	60A
20	186
50	240
100	430

The diffraction lines due to the mixtures were abnormal in shape being obviously the result of the superposition of two lines of the shape ordinarily observed. This is evidence that each of the Pt. Blacks used is relatively uniform in size. It also suggests that the shape of a diffraction line can be used as a qualitative criterion of the uniformity of an unknown sample.

IV. Concluding Remarks

The experiments reported indicate that in many cases the results obtained may err by a factor of 2 in absolute value though it appears that relative estimates of particle-size on similar materials may have considerable significance even when some of the refinements are dispensed with. It is probable that the question of particle-size distribution can be overlooked at the present time although determinations on materials which have been prepared under controlled conditions can obviously be relied on to a greater de-

gree than when the history of the material is quite unknown. This paper has not touched on the problem of lattice distortion, although most of the materials worked with have been prepared under such conditions that this source of trouble might be expected to be minimized.

Further work, both theoretical and experimental, is obviously indicated, especially with regard to the total absorption method of Brill and Pelzer which is preferable to the others, particularly if the theoretical treatment can be carried through more rigorously.

The writer wishes to express his appreciation of the many helpful discussions with Dr. A. L. Patterson of the Johnson Foundation, University of Pennsylvania, and with Dr. A. W. Kenney of this laboratory who suggested the study. Thanks are also due Dr. J. B. Nichols for his ultra-centrifuge work and Mr. H. Aughey for skillful technical assistance.

Thickness Vibrations of Piezoelectric Oscillating Crystals

By Issac Koga
Tokyo University of Engineering

(Received April 4, 1932)

For several years, it has been well known that, in the natural vibration of a piezoelectric oscillating crystal, there is a certain period proportional only to the thickness, but, so far as we are aware, there has been no concrete explanation for this vibration nor how its period is connected with the physical constants of the medium. The present paper shows that such a vibration, named *thickness vibration* for brevity, is due to the standing wave produced by interference of plane waves incident to and reflected from the plane boundary surfaces of the medium, and verifies the theoretical results by several examples. There are three normal modes in the thickness vibration, and the corresponding frequencies are given in first approximation by a representative formula: $P/2\pi=(q/2a)\ (c/\rho)^{1/2}$, where q is any integer, a the thickness of the plate, ρ the density and c a certain adiabatic elastic constant depending upon the orientation of the plate with respect to the crystallographic axes of the medium. It is not always possible to excite all normal modes of vibration piezoelectrically. The electrically measured natural frequency of the thickness vibration is always a little higher than that calculated by the formula. Adiabatic elastic constants of piezoelectric crystals may be determined in first approximation by measurement of the frequencies of thickness vibrations of plates prepared from given crystals.

I. Introduction

As IS well known, a thin piezoelectric crystal plate has in general many modes of vibration, but the shortest period of fundamental vibration is always dependent only upon the thickness of the plate. We shall name this vibration the *thickenss vibration*.

Although many papers have been published upon the vibration of piezoelectric crystal, none has yet pointed out clearly, as far as we are aware, that the thickness vibration of thin crystal plate is a mere result of standing waves produced by the interference of plane waves, the wave surfaces of which are parallel to the boundary surfaces.

II. Equations of Motions in Crystalline Media

The fundamental period of the thickness vibration of a very thin crystal plate is dependent almost entirely upon the thickness of the plate, so that we may consider the extent of the surfaces to be infinite.

The free vibration of a thin crystal plate having two parallel plane boundary surfaces is due to the interference of plane waves incident to and reflected from those boundary surfaces. In other words, in the thickness vibration of the crystal plate bounded by the two infinite parallel planes $x=0$ and $x=a$, the displacement at any point in the medium is dependent only upon x and t, and not upon y and z. Therefore the general equations of motions in a crystalline medium,

$$\left.\begin{aligned} \partial X_x/\partial x + \partial X_y/\partial y + \partial X_z/\partial z &= \rho\partial^2 u/\partial t^2, \\ \partial Y_x/\partial x + \partial Y_y/\partial y + \partial Y_z/\partial z &= \rho\partial^2 v/\partial t^2 \\ \partial Z_x/\partial x + \partial Z_y/\partial y + \partial Z_z/\partial z &= \rho\partial^2 w/\partial t^2, \end{aligned}\right\} \tag{1}$$

where

$$\left.\begin{aligned} X_x &= c_{11}e_{xx} + c_{12}e_{yy} + c_{13}e_{zz} + c_{14}e_{yz} + c_{15}e_{zx} + c_{16}e_{xy}, \\ &\cdots\cdots\cdots\cdots\cdots\cdots\cdots\cdots \\ X_y &= c_{61}e_{xx} + c_{62}e_{yy} + c_{63}e_{zz} + c_{64}e_{yz} + c_{65}e_{zx} + c_{66}e_{xy}, \\ c_{hk} &= c_{kh}, \\ e_{xx} &= \frac{\partial u}{\partial x}, \quad e_{yy} = \frac{\partial v}{\partial y}, \quad e_{zz} = \frac{\partial w}{\partial z}, \\ e_{yz} &= \frac{\partial w}{\partial y} + \frac{\partial v}{\partial z}, \quad e_{zx} = \frac{\partial u}{\partial z} + \frac{\partial w}{\partial x}, \quad e_{xy} = \frac{\partial v}{\partial x} + \frac{\partial u}{\partial y}, \end{aligned}\right\} \tag{2}$$

u, v, w, displacement in the direction of x, y, z respectively, ρ, density of the medium, reduce to the very simple forms:

$$\left.\frac{\partial X_x}{\partial x} = \rho\frac{\partial^2 u}{\partial t^2}, \quad \frac{\partial Y_x}{\partial x} = \rho\frac{\partial^2 v}{\partial t^2}, \quad \frac{\partial Z_x}{\partial x} = \rho\frac{\partial^2 w}{\partial t^2}, \right\} \tag{3}$$

or further

$$\left.\begin{aligned} (\partial^2/\partial x^2)(c_{11}u + c_{16}v + c_{15}w) &= \rho\partial^2 u/\partial t^2, \\ (\partial^2/\partial x^2)(c_{16}u + c_{66}v + c_{56}w) &= \rho\partial^2 v/\partial t^2, \\ (\partial^2/\partial x^2)(c_{15}u + c_{56}v + c_{55}w) &= \rho\partial^2 w/\partial t^2. \end{aligned}\right\} \tag{4}$$

Now let l, m, n and c be so chosen that

$$\left.\begin{aligned} lc_{11} + mc_{16} + nc_{15} &= lc \\ lc_{16} + mc_{66} + nc_{56} &= mc \\ lc_{15} + mc_{56} + nc_{55} &= nc \end{aligned}\right\} \tag{5}$$

and put

$$\xi = lu + mv + nw, \tag{6}$$

then, multiplying the three equations of (4) by l, m, n and adding together, we have in the most compact form:

$$\partial^2\xi/\partial t^2 = (c/\rho)(\partial^2\xi/\partial x^2). \tag{7}$$

Eliminating l, m, n between the three equations of (5), we have

$$\begin{vmatrix} c_{11} - c & c_{16} & c_{15} \\ c_{16} & c_{66} - c & c_{56} \\ c_{15} & c_{56} & c_{55} - c \end{vmatrix} = 0 \tag{8}$$

a cubic equation determining c; let its roots, which are proved to be necessarily real and positive,[1] be c_1, c_2, c_3. When c_1 is substituted in any two of the foregoing equations, the ratios of $l:m:n$ can be derived; let them be denoted

[1] Lord Kelvin, Baltimore Lectures, London, 1904.

by $l_1:m_1:n_1$, and suppose the corresponding value of ξ to be ξ_1 with similar expressions for the other values of c. Then ξ_1, ξ_2, and ξ_3 are always proved to be perpendicular to each others.

The solution of (7) is a very simple matter. To determine the normal mode of vibration we must assume that ξ varies as a harmonic function of the time t

$$\xi \propto e^{ipt}. \tag{9}$$

Then as a function of x, ξ must satisfy

$$d^2\xi/dx^2 + (p^2\rho/c)\xi = 0 \tag{10}$$

of which the complete integral is

$$\xi = A \cos [px(\rho/c)^{1/2}] + B \sin [px(\rho/c)^{1/2}] \tag{11}$$

where A and B are independent of x.

Now when both boundary surfaces are free from tractions,

$$X_x = Y_x = Z_x = 0 \text{ or } \partial\xi/\partial x = 0 \text{ at } x = 0 \text{ and } x = a, \tag{12}$$

we get

$$B = 0 \text{ and } \sin [pa(\rho/c)^{1/2}] = 0 \tag{13}$$

from which

$$p/2\pi = (q/2a)(c/\rho)^{1/2} \tag{14}$$

q being integral.

Accordingly, the normal mode is given by equation of the form

$$\xi = A \cos (q\pi x/a) \cdot e^{ipt} \tag{15}$$

where A is an arbitrary constant, which may be determined in the usual manner, when the initial value of ξ is given.

Similarly if the medium be bounded by two parallel planes $y=0$ and $y=a$, we may replace (5), (8) and (15) by

$$lc_{66} + mc_{26} + nc_{46} = lc;\ lc_{26} + mc_{22} + nc_{24} = mc;\ lc_{46} + mc_{24} + nc_{44} = nc. \tag{16}$$

$$\begin{vmatrix} c_{66} - c & c_{26} & c_{46} \\ c_{26} & c_{22} - c & c_{24} \\ c_{46} & c_{24} & c_{44} - c \end{vmatrix} = 0 \tag{17}$$

$$\xi = A \cos (q\pi y/a) \cdot e^{ipt} \tag{18}$$

and if the medium be bounded by $z=0$ and $z=a$, by

$$lc_{55} + mc_{45} + nc_{35} = lc;\ lc_{45} + mc_{44} + nc_{34} = mc;\ lc_{35} + mc_{34} + nc_{33} = nc. \tag{19}$$

$$\begin{vmatrix} c_{55} - c & c_{45} & c_{35} \\ c_{45} & c_{44} - c & c_{34} \\ c_{35} & c_{34} & c_{33} - c \end{vmatrix} = 0 \tag{20}$$

$$\xi = A \cos (q\pi z/a) \cdot e^{ipt}. \tag{21}$$

It is well known that we can excite one or more of the free thickness vibrations by applying an alternating electric field of suitable frequency in the direction normal to the boundary surfaces of crystal, provided the crystal plate is prepared so that it is piezoelectrically active; and also that it is sometimes possible to sustain a continuous oscillation by properly employing the thermionic tube circuit. The ease of maintenance depends considerable upon the medium and the orientation of the boundary surfaces.

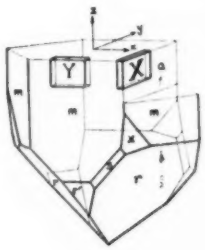

Fig. 1.

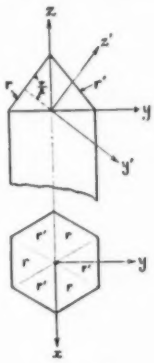

Fig. 2.

III. Thickness Vibration of Quartz Plate

Of the piezoelectric crystals, quartz is the most familiar to high-frequency engineers, so that we may first verify the theory with this medium. In quartz, if the coordinate axes be chosen as in Fig. 1, the adiabatic elastic constants[2] and density are as follows:

$$\left.\begin{aligned} c_{11} &= 85.45 \times 10^{10}\ \text{dynes/cm}^2, & c_{12} &= 7.26 \times 10^{10}\ \text{dynes/cm}^2, \\ c_{33} &= 105.67 \times 10^{10}\ \text{dynes/cm}^2, & c_{13} &= 14.37 \times 10^{10}\ \text{dynes/cm}^2, \\ c_{44} &= 57.09 \times 10^{10}\ \text{dynes/cm}^2, & -c_{14} &= 16.87 \times 10^{10}\ \text{dynes/cm}^2, \\ & \rho = 2.654\ \text{grams/cm}^3, \end{aligned}\right\} \tag{22}$$

while the relations between applied electric fields and strains are:

$$\left.\begin{aligned} e_{xx} &= d_{11}E_x, & e_{zz} &= -d_{14}E_y, \\ e_{yy} &= -d_{11}E_x, & e_{xy} &= -2d_{11}E_y, \\ e_{yz} &= d_{14}E_x, & & \\ d_{11} &= 6.45 \times 10^{-8}\ \text{C.G.S. units}, & & \\ -d_{14} &= 1.45 \times 10^{-8}\ \text{C.G.S. units}. & & \end{aligned}\right\} \tag{23}$$

(1) In X-cut quartz plate designated by X in Fig. 1, if the boundary surfaces be expressed by $x=0$ and $x=a$, (8) reduces to

$$\begin{vmatrix} c_{11}-c & 0 & 0 \\ 0 & \frac{1}{2}(c_{11}-c_{12})-c & c_{14} \\ 0 & c_{14} & c_{44}-c \end{vmatrix} = 0 \tag{24}$$

[2] W. Voigt, Lehrbuch der Kristallphysik, 754 and 789 (1928).

or

$$\left.\begin{aligned} c_1 &= c_{11} = 85.45 \times 10^{10}\ \text{dynes/cm}^2, \\ c_2, c_3 &= \tfrac{1}{4}(c_{11} - c_{12}) + \tfrac{1}{2}c_{44} \pm \left[\left\{\tfrac{1}{4}(c_{11} - c_{12}) - \tfrac{1}{2}c_{44}\right\}^2 + c_{14}^2\right]^{1/2} \\ c_2 &= 67.22 \times 10^{10}\ \text{dynes/cm}^2, \\ c_3 &= 28.98 \times 10^{10}\ \text{dynes/cm}^2, \end{aligned}\right\} \quad (25)$$

and the ratio $l:m:n$ corresponding to these values:

$$\left.\begin{aligned} l_1 : m_1 : n_1 &= 1:0:0, \\ l_2 : m_2 : n_2 &= 0 : c_2 - c_{44} : c_{14} = 0 : -0.60 : 1, \\ l_3 : m_3 : n_3 &= 0 : c_3 - c_{44} : c_{14} = 0 : 1.67 : 1. \end{aligned}\right\} \quad (26)$$

The normal modes of vibration are given by the following equations:

$$\xi = A \cos(q\pi x/a) \cdot e^{ipt}, \quad (27)$$

where $\xi_1 = u$; $\xi_2 = -0.60\ v + w$; and $\xi_3 = 1.67\ v + w$; while the electric field in the direction x cannot excite the displacement ξ_2 and ξ_3 as is seen from (23), so that the period of vibration is

$$p/2\pi = (q/2a)(c_{11}/\rho)^{1/2} = q/a \times 0.2837 \times 10^6\ \text{cycles/sec.}, \quad (28)$$

and the mode of vibration is

$$u = A \cos(q\pi x/a) e^{ipt} \quad (29)$$

that is, the pure longitudinal vibration along the normal to the surfaces.

As an experimental example, a quartz oscillating crystal 0.0922 $\times$2.610 $\times$2.684 cm^3 (the normal to the major surfaces inclines 7′ the axis x) had the fundamental frequency of thickness vibration 3.10×10^6 cycles/sec., from from which we get

$$p/2\pi = (1/a) + 0.0922 \times 3.10 \times 10^6 = (1/a) \times 0.286 \times 10^6\ \text{cycles/sec.}, \quad (30)$$

which is seen to be very near upon the theoretical result (28).

(2) In Y-cut quartz plate designated by Y in Fig. 1, if the boundary surfaces be expressed by $y = 0$ and $y = a$, (17) reduces to

$$\begin{vmatrix} \tfrac{1}{2}(c_{11} - c_{12}) - c & 0 & 0 \\ 0 & c_{11} - c & -c_{14} \\ 0 & -c_{14} & c_{44} - c \end{vmatrix} = 0 \quad (31)$$

or

$$\left.\begin{aligned} c_1 &= \tfrac{1}{2}(c_{11} - c_{12}) = 39.10 \times 10^{10}\ \text{dynes/cm}^2, \\ c_2, c_3 &= \tfrac{1}{2}(c_{11} + c_{44}) \pm \left[\tfrac{1}{4}(c_{11} - c_{44})^2 + c_{14}^2\right]^{1/2} \\ c_2 &= 93.31 \times 10^{10}\ \text{dynes/cm}^2, \\ c_3 &= 49.23 \times 10^{10}\ \text{dynes/cm}^2, \end{aligned}\right\} \quad (32)$$

and the ratio $l:m:n$ corresponding to these values:

$$\left.\begin{aligned} l_1 : m_1 : n_1 &= 1:0:0 \\ l_2 : m_2 : n_2 &= 0 : c_{44} - c_2 : c_{14} = 0:2.15:1 \\ l_3 : m_3 : n_3 &= 0 : c_{44} - c_3 : c_{14} = 0: -0.47:1 \end{aligned}\right\} \tag{33}$$

The normal modes of vibration are given by

$$\xi = A \cos(q\pi y/a) \cdot e^{ipt} \tag{34}$$

where $\xi_1 = u$, $\xi_2 = 2.15\, v + w$, and $\xi_3 = -0.47\, v + w$, of which ξ_2 and ξ_3 cannot be excited piezoelectrically by the electric field in the direction of y axis as is clear from (23), so that the displacement is given by

$$u = A \cos(q\pi y/a) \cdot e^{ipt} \tag{35}$$

which shows that the vibration is of a pure shear as is pointed out by Professor Cady.[3]

The frequency of vibration is

$$\frac{p}{2\pi} = \frac{q}{2a}\left(\frac{c_{11} - c_{12}}{2\rho}\right)^{1/2} = \frac{q}{a} \times 0.1919 \times 10^6 \text{ cycles/sec.}, \tag{36}$$

while in the experiment with a sample $0.1909 \times 3.200 \times 3.304$ cm^3 (the normal to the major surfaces inclines 6′ to the axis y) the fundamental frequency of thickness vibration is 1.02×10^6 cycles/sec., that is

$$p/2\pi = 1/a + 0.1909 \times 1.02 \times 10^6 = 1/a \times 0.195 \times 10^6 \text{ cycles/sec.}, \tag{37}$$

which is also seen to be very near upon the theoretical result (36).

(3) In quartz plate cut parallel to a surface of positive rhombohedron designated by r in Fig. 1 (say R-cut plate[4]), the vibration is observed to be extremely vigorous and the third harmonic vibration ($q = 3$) can often be sustained by Pierce circuit,[5] in which an oscillating crystal plate is placed between grid and filament of a three-electrode thermionic tube.

To obtain periods and normal modes of thickness vibration, we may first transfer the coordinate axes. Let x', y', z', be so chosen that the direction cosines of them referred to the original axes be expressed by the orthogonal scheme

	x	y	z
x'	1	0	0
y'	0	$\cos\theta$	$-\sin\theta$
z'	0	$\sin\theta$	$\cos\theta$

(38)

where

$$\theta = \arctan(3^{1/2}/2.200), \tag{39}$$

[3] W. G. Cady, A shear mode of crystal vibration, Phys. Rev. **29**, 617A (1927).

[4] I. Koga, R-cut quartz oscillating crystal plate and the harmonic vibration, Supplementary Issue, Jour. I.E.E. (Japan) to be issued in April (1932).

[5] G. W. Pierce, Piezoelectric crystal resonators and crystal oscillators applied to the precision calibration of wave meters, Proc. A.A.A.S. **59**, 81–106 (1923).

then the axis y' becomes normal to the surface r as shown in Fig. 2. If the elastic constants referred to the new axes be denoted by c'_{hk}, values of c's in (14) are the roots of

$$\begin{vmatrix} c_{66}' - c & 0 & 0 \\ 0 & c_{22}' - c & c_{24}' \\ 0 & c_{24}' & c_{44}' - c \end{vmatrix} = 0 \tag{40}$$

or

$$\left.\begin{aligned} c_1 = c_{66}' &= c_{44}\sin^2\theta + \tfrac{1}{2}(c_{11} - c_{12})\cos^2\theta - c_{14}\sin 2\theta \\ &= 62.39 \times 10^{10}\ \text{dynes/cm}^2, \\ c_2, c_3 &= \tfrac{1}{2}(c_{22}' + c_{44}') \pm [\tfrac{1}{4}(c_{22}' - c_{44}')^2 + c_{24}'^2]^{1/2} \end{aligned}\right\} \tag{41}$$

and the ratio $l:m:n$ corresponding to these values:

$$\left.\begin{aligned} l_1 : m_1 : n_1 &= 1:0:0 \\ l_2 : m_2 : n_2 &= 0 : c_{44}' - c_2 : c_{24}' \\ l_3 : m_3 : n_3 &= 0 : c_{44}' - c_3 : c_{24}' \end{aligned}\right\} \tag{42}$$

The normal modes of vibration are given by

$$\xi = A\cos(q\pi y'/a)\cdot e^{ipt} \tag{43}$$

where $\xi_1 = u'$, $\xi_2 = (c_{44}' - c_2)\,v' + c_{24}'w'$, $\xi_3 = (c_{44}' - c_3)\,v' + c_{24}'w'$. On the other hand, the relations (24) transform into the following relations:

$$\left.\begin{aligned} e_{x'x'} &= d_{11}E_{x'}, \\ e_{y'y'} &= -\cos\theta(d_{11}\cos\theta + d_{14}\sin\theta)E_{x'}, \\ e_{z'z'} &= -\sin\theta(d_{11}\sin\theta + d_{14}\cos\theta)E_{x'}, \\ e_{y'z'} &= (d_{11}\sin 2\theta + d_{14})E_{x'}, \\ e_{z'x'} &= -(d_{14}\cos\theta - 2d_{11}\sin\theta)(E_{y'}\cos\theta + E_{z'}\sin\theta), \\ e_{x'y'} &= (d_{14}\sin\theta - 2d_{11}\cos\theta)(E_{y'}\cos\theta + E_{z'}\sin\theta), \end{aligned}\right\} \tag{44}$$

from which we see that we cannot excite the displacements ξ_2 and ξ_3 by the electric field along the axis y', consequently the displacement is given by

$$u' = A\cos(q\pi y'/a)\cdot e^{ipt} \tag{45}$$

which shows that the mode of vibration is of a pure shear. The frequency of vibration is

$$p/2\pi = (q/2a)(c_{66}'/\rho)^{1/2} = q/a \times 0.2424 \times 10^6\ \text{cycles/sec.}, \tag{46}$$

while in the experiment with a sample $0.1002 \times 2.592 \times 2.762$ cm^3 (the normal to the major surfaces inclines within $1'$ to the axis y') the fundamental frequency of thickness vibration is 2.47×10^6 cycles/sec., that is

$$p/2\pi = 1/a \times 0.1002 \times 2.47 \times 10^6 = 1/a \times 0.247 \times 10^6\ \text{cycles/sec.}, \tag{47}$$

which is also seen to be very near the theoretical result (46).

There have been published several papers[6] on the excitation of harmonic vibrations in a resonator, but as far as we are aware, very little work has been done on the harmonics of the thickness vibration of a crystal. The present crystal plate can often be sustained in its first and third harmonic vibrations separately by the Pierce circuit above mentioned. Fig. 3 shows the characteristic features of the oscillator. The higher frequency of the vibrations is easily observed by a heterodyne frequency-meter to be just three times that of the lower.

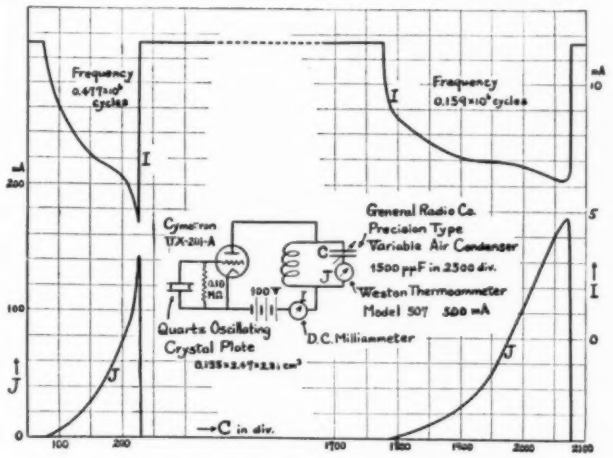

Fig. 3.

Examples of dimensions which are suited for the third harmonic vibrations are:

Dimensions (cm^3)	Approx. frequency of vibrations (cycles/sec.)
$0.093 \times 2.56 \times 2.57$	2.66×10^6 and $2.66 \times 10^6 \times 3$
$0.114 \times 2.09 \times 2.70$	2.17×10^6 and $2.17 \times 10^6 \times 3$
$0.155 \times 2.47 \times 2.81$	1.59×10^6 and $1.59 \times 10^6 \times 3$
$0.185 \times 2.77 \times 2.98$	1.34×10^6 and $1.34 \times 10^6 \times 3$.

(48)

(Inclinations of the major surfaces to the $x'z'$ plane are generally not greater than 10′).

(4) If the boundary surfaces are parallel to surfaces of a negative rhombohedron designated by r' in Fig. 1, normal modes and frequencies of vibration can be studied as in the previous case. The only difference is the reversal of the sign of θ in Fig. 2. Thus

$$\begin{aligned} c_{66}' &= c_{44}\sin^2\theta + \tfrac{1}{2}(c_{11} - c_{12})\cos^2\theta + c_{14}\sin 2\theta \\ &= 29.59 \times 10^{10}\ \text{dynes/cm}^2, \end{aligned} \tag{49}$$

and

$$p/2\pi = (q/2a)(c_{66}'/\rho)^{1/2} = q/a \times 0.1670 \times 10^6\ \text{cycles/sec.} \tag{50}$$

[6] E. Giebe and A. Scheibe, Sichtbarmachung von hochfrequenten Longitudinalschwingungen piezo-elektrischer Kristallstaebe, Zeits. f. Physik **33,** 335 (1925).

The displacement

$$u' = A \cos (q\pi y'/a) \cdot e^{ipt} \tag{51}$$

gives a pure shear vibration.

From the experiment with a sample $0.0765 \times 2.76 \times 3.19$ cm^3 (the normal to the major surfaces inclines 5′ to the axis y') the frequency of vibration is 2.20×10^6 cycles/sec., that is

$$p/2\pi = 1/a \times 0.0765 \times 2.20 \times 10^6 = 1/a \times 0.168 \times 10^6 \text{ cycles/sec.}, \tag{52}$$

which is very near the theoretical result (50).

It is seen above that the frequency of vibration of a piezoelectric oscillating crystal is always a little higher than that calculated from the elastic constants. This small difference must be, to a certain extent, due to the finiteness of the boundary surfaces of plate, but it is not overlooked that the frequency of pure mechanical vibration is different from that as a piezoelectric oscillating crystal. In fact, when the crystal plate is excited to vibrate with its natural vibration, the equivalent elastic constants become slightly greater than that which is determined elastostatically. For example, by a strain e_{xx}, besides the stress $c_{11}e_{xx}$, the polarization of $\epsilon_{11}e_{xx}$ is produced, ϵ_{11} being the piezoelectric constant, so that the crystal, being acted upon by the electric field $4\pi\epsilon_{11}e_{xx}/K$, where K is the dielectric constant, has a stress $4\pi\epsilon_{11}^2e_{xx}/K$, which adds to the above-mentioned stress $c_{11}e_{xx}$. Consequently the resultant adiabatic elastic constant c_{11}^0 becomes

$$c_{11}^0 = c_{11} + \frac{4\pi\epsilon_{11}^2}{K} = c_{11}\left\{1 + \frac{4\pi \times (4.77 \times 10^4)^2}{85.45 \times 10^{10} \times 4.5}\right\} = c_{11}(1 + 0.0074). \tag{53}$$

In other words, to replace a quartz oscillating crystal by an equivalent electrical network,[7] we must, as shown in Fig. 4, consider C_1, which represents the capacity of the quartz as a mere dielectric, parallel to the series resonance

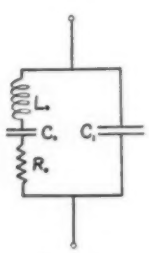

Fig. 4.

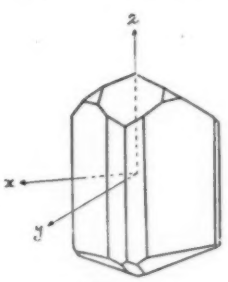

Fig. 5.

circuit L_0, C_0, R_0 representing the mechanical vibrating system. If such is the case, we can easily understand that the electrically measured natural frequency of vibration determined by L_0, C_0, C_1, is always higher than that determined by L_0, C_0. The ratio $C_0:C_1$, is in general, not greater than 1/100.

[7] D. W. Dye, Piezoelectric quartz resonator and equivalent electrical circuit, Proc. Phys. Soc. London **38**, 399–457 (1926).

IV. Thickness Vibration of Tourmaline Plate

Tourmaline is not yet widely used as a piezoelectric oscillating crystal, and we have no occasion to investigate by fine crystal, but we can foresee the normal modes and frequencies of vibration in the first approximation.

The adiabatic elastic constants referred to the coordinate axes shown in Fig. 5 are composed of the same scheme with (22), the numerical values being

$$\left.\begin{aligned} c_{11} &= 270.17 \times 10^{10}\ \text{dynes/cm}^2, & c_{12} &= 69.06 \times 10^{10}\ \text{dynes/cm}^2, \\ c_{33} &= 160.69 \times 10^{10}\ \text{dynes/cm}^2, & c_{13} &= 8.83 \times 10^{10}\ \text{dynes/cm}^2, \\ c_{44} &= 66.71 \times 10^{10}\ \text{dynes/cm}^2, & -c_{14} &= 7.75 \times 10^{10}\ \text{dynes/cm}^2, \\ & \rho = 3.100\ \text{grams/cm}^3 & & \end{aligned}\right\} \quad (54)$$

while the relations between electric fields and strains are:

$$\left.\begin{aligned} e_{xx} &= -d_{22}E_y + d_{31}E_z, & e_{yz} &= d_{15}E_y, \\ e_{yy} &= d_{22}E_y + d_3E_z, & e_{zx} &= d_{15}E_x, \\ e_{zz} &= d_{33}E_z, & e_{xy} &= -2d_{22}E_x, \\ -d_{22} &= 0.69 \times 10^{-8}\ \text{C.G.S. units}, & d_{31} &= 0.74 \times 10^{-8}\ \text{C.G.S. units} \\ d_{33} &= 5.78 \times 10^{-8}\ \text{C.G.S. units}, & d_{15} &= 11.04 \times 10^{-8}\ \text{C.G.S. units} \end{aligned}\right\} \quad (55)$$

(1) If the boundary surfaces of plate be $z=0$ and $z=a$, (20) reduces to

$$\begin{vmatrix} c_{44}-c & 0 & 0 \\ 0 & c_{44}-c & 0 \\ 0 & 0 & c_{33}-c \end{vmatrix} = 0 \quad (56)$$

or

$$\left.\begin{aligned} c_1 &= c_2 = c_{44} = 66.71 \times 10^{10}\ \text{dynes/cm}^2, \\ c_3 &= c_{33} = 160.69 \times 10^{10}\ \text{dynes/cm}^2, \end{aligned}\right\} \quad (57)$$

and the ratio $l:m:n$ corresponding to these values:

$$\left.\begin{aligned} l_1 : m_1 : n_1 &= 1:0:0 \\ l_2 : m_2 : n_2 &= 0:1:0 \\ l_3 : m_3 : n_3 &= 0:0:1 \end{aligned}\right\} \quad (58)$$

The normal modes of vibration are given by the following equations:

$$\left.\begin{aligned} \xi_1 &= u = A\cos(q\pi x/a)\cdot e^{ipt}, \\ \xi_2 &= v = A\cos(q\pi x/a)\cdot e^{ipt}, \\ \xi_3 &= w = A\cos(q\pi x/a)\cdot e^{ipt}, \end{aligned}\right\} \quad (59)$$

of which w can only be excited piezoelectrically by the electric field along the axis z, as is seen from (55). Accordingly the vibration is of a pure longitudinal. The corresponding frequency of vibration is

$$p/2\pi = (q/2a)(c_{33}/\rho)^{1/2} = (q/a) \times 0.3600 \times 10^6\ \text{cycles/sec}. \quad (60)$$

(2) If the boundary surfaces of plate be $x=0$ and $x=a$, (8) reduces to

$$\begin{vmatrix} c_{11}-c & 0 & 0 \\ 0 & \frac{1}{2}(c_{11}-c_{12})-c & c_{14} \\ 0 & c_{14} & c_{44}-c \end{vmatrix} = 0 \tag{61}$$

or

$$\left.\begin{aligned} c_1 &= c_{11} = 270.17 \times 10^{10}\ \text{dynes/cm}^2, \\ c_2, c_3 &= \tfrac{1}{4}(c_{11}-c_{12}) + \tfrac{1}{2}c_{44} \pm [\{\tfrac{1}{4}(c_{11}-c_{12}) - \tfrac{1}{2}c_{44}\}^2 + c_{14}^2]^{1/2} \\ c_2 &= 102.25 \times 10^{10}\ \text{dynes/cm}^2, \\ c_3 &= 65.03 \times 10^{10}\ \text{dynes/cm}^2, \end{aligned}\right\} \tag{62}$$

and the ratio $l:m:n$ corresponding to these values:

$$\left.\begin{aligned} l_1:m_1:n_1 &= 1:0:0 \\ l_2:m_2:n_2 &= 0:c_2-c_{44}:c_{14} = 0:-4.59:1 \\ l_3:m_3:n_3 &= 0:c_3-c_{44}:c_{14} = 0:0.22:1 \end{aligned}\right\} \tag{63}$$

The normal modes of vibration are given by the following equations:

$$\xi = A\cos(q\pi x/a)\cdot e^{ipt} \tag{64}$$

where $\xi_1=u$, $\xi_2=-4.59\ v+w$, $\xi_3=0.22\ v+w$, while the electric field in the direction x cannot excite the displacement ξ_1 and can hardly excite ξ_2 as is seen from (56), and the periods of ξ_2 and ξ_3 are:

$$p/2\pi = (q/2a)(c_2/\rho)^{1/2} = q/a \times 0.2872 \times 10^6\ \text{cycles/sec.}, \tag{65}$$

$$p/2\pi = (q/2a)(c_3/\rho)^{1/2} = q/a \times 0.2290 \times 10^6\ \text{cycles/sec.} \tag{66}$$

Resistance-Temperature Relation of Beryllium Oxide and Zinc Oxide

By JOHN A. OSTEEN
Department of Physics, Lehigh University

(Received June 13, 1932)

Bidwell showed that the resistance-temperature law for certain variable conductors (oxides, etc.) was of the form $\rho = Ae^{Q/RT+aT}$. Plotted in the form $(1/\rho)(d\rho/dT) = Q/RT^2 - a$ he obtained for Fe_2O_3 straight lines with a break near the recalescence point, the two lines having the same y intercept but different slopes. This law was also followed by metallic germanium. The present paper extends this work to zinc oxide and beryllium oxide. Beryllium oxide yields a straight line showing a transition at 750°C. Zinc oxide yields two straight lines with a transition in the interval 250°C–500°C. The two zinc oxide lines have different slopes but the same y intercepts. With successive heatings to 1050°C there occurs continued decreases in the slope of the line for the 500°C–1000°C range but no change in the y intercept. The line for the range 0°C–250°C changes on successive heatings to 1050°C and finally stabilizes to a value of slope and intercept which repeats on succeeding runs. On the suggesion that the indicated transformation was due to impurity, new material of special purity prepared by the New Jersey Zinc Company was studied. The behavior of this material was found to agree closely with that of the earlier specimen but gave a more clean cut transformation.

INTRODUCTION

KÖNIGSBERGER[1] on the basis of the electron theory of Drude derived, by making use of certain empirical relations, the expression

$$\rho = A(1 + \alpha t + \beta t^2)e^{Q/RT} \tag{1}$$

for the resistance of variable conductors. (ρ) is the specific resistance (used in this work as total resistance); (t) the temperature on the centigrade scale; (T) the temperature on the absolute scale; (R) the gas constant (approximately 2); (Q) the heat of dissociation of the electrons, i.e., the heat required to liberate a gram-atom of electrons from the atoms to which they are supposed to be bound; (e) the Naperian base; (A), (α), and (β), constants.

In the case of Fe_2O_3 Bidwell[2] showed that the resistance-temperature relation could be written in the form

$$\rho = Ae^{Q/RT+aT}. \tag{2}$$

Eq. (2) differs from (1) in that the exponential e^{aT} is substituted for $(1+\alpha t+\beta t^2)$. This proved to be empirically satisfactory and more convenient than (1) for graphical testing.

By expressing Eq. (2) in the form

$$\log_{10}\rho = 0.435(Q/RT + aT) + \log_{10} A \tag{3}$$

and differentiating, we have

[1] Königsberger, Ann. d. Physik **32**, 179 (1910).
[2] Bidwell, Phys. Rev. (2) **8**, 12 (1916).

$$[-(1/\rho)(d\rho/dT)] = Q/RT^2 - a. \qquad (4)$$

If a straight line is obtained by plotting the left hand member of Eq. (4) as ordinate against $1/T^2$ as abscissa, the equation is verified.

Bidwell obtained for Fe_2O_3 straight lines with a break in the 600°C to 800°C region. This break he relates to the recalescence point in iron which occurs in this region. The present paper offers some results for the resistance-temperature relations for specimens of BeO and ZnO as plotted by the above method. In addition, for comparison, logarithmic plots, similar to those usually made for variable conductors are also included.[3]

Preparation of Specimens and Methods Employed

The materials used were C.P. BeO prepared at Cornell University; Bakers C.P. ZnO and S.P. ZnO prepared by the New Jersey Zinc Company.

Data were obtained on compressed and baked specimens prepared as explained by Bidwell for iron oxide.[2]

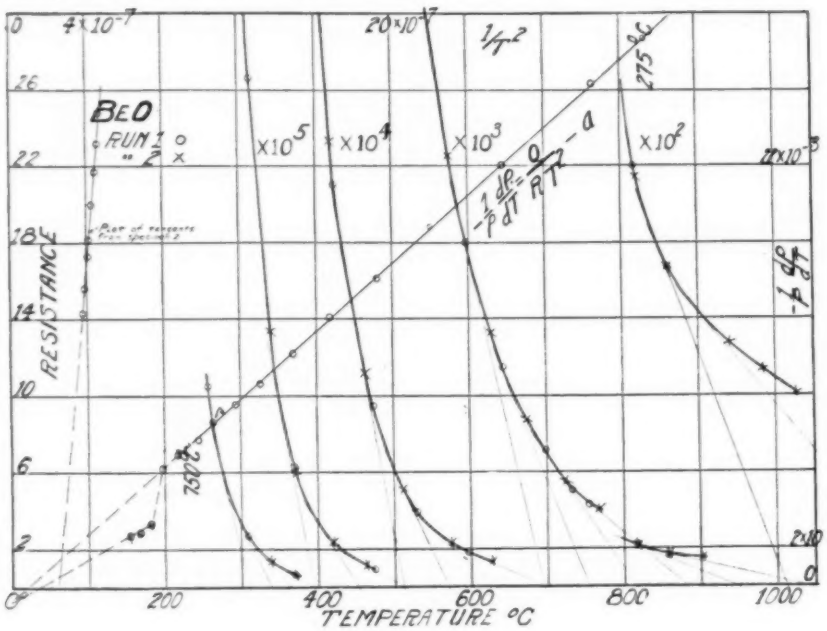

Fig. 1.

Discussion of Data for BeO

Fig. 1 shows for two runs on the specimen of BeO resistance plotted directly against temperature. The resistance value at any point is obtained by multiplying the reading taken on the resistance-axis by the indicated power of 10 of the curve from which the point is taken. The heating interval between runs (1) and (2) did not affect the absolute values as is seen in the coincidence of the curves. From this curve, tangents were drawn as shown and with the data thus obtained Eq. (4) was plotted. This gave a straight line from 275°C to 750°C. The value of Q (17,800) from this line is of the order of values re-

[3] Spanner, Ann. d. Physik **75**, 609 (1924).

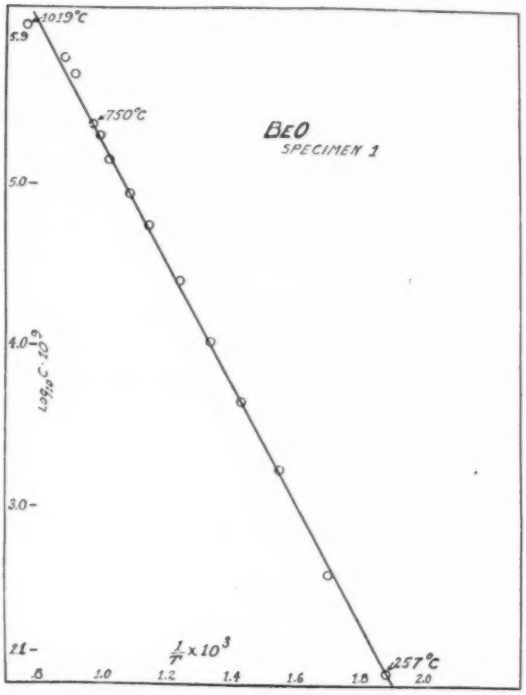
1019°C
750°C
BeO
SPECIMEN 1
257°C
5.9
5.0
4.0
3.0
2.1
.8
1.0
1.2
1.4
1.6
1.8
2.0

Fig. 2.

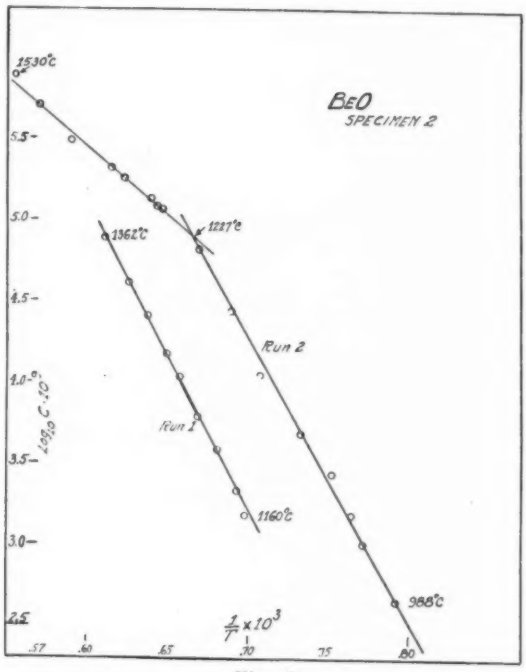
1530°C
BeO
SPECIMEN 2
1227°C
1362°C
Run 2
Run 1
1160°C
988°C
5.5
5.0
4.5
3.5
3.0
2.5
.57
.60
.65
.70
.75
.80

Fig. 3.

ported by Königsberger for CuO, SiO_2, ThO and CeO, as well as near the value 17,400 obtained by Bidwell for Fe_2O_3.

The noticeable lack of smoothness in the resistance-temperature curve between 750°C and 800°C is followed, in the plot of Eq. (4) by a transition the last three points of which indicate another possible straight line with resistance intercept of same value as the 275°C to 750°C line.

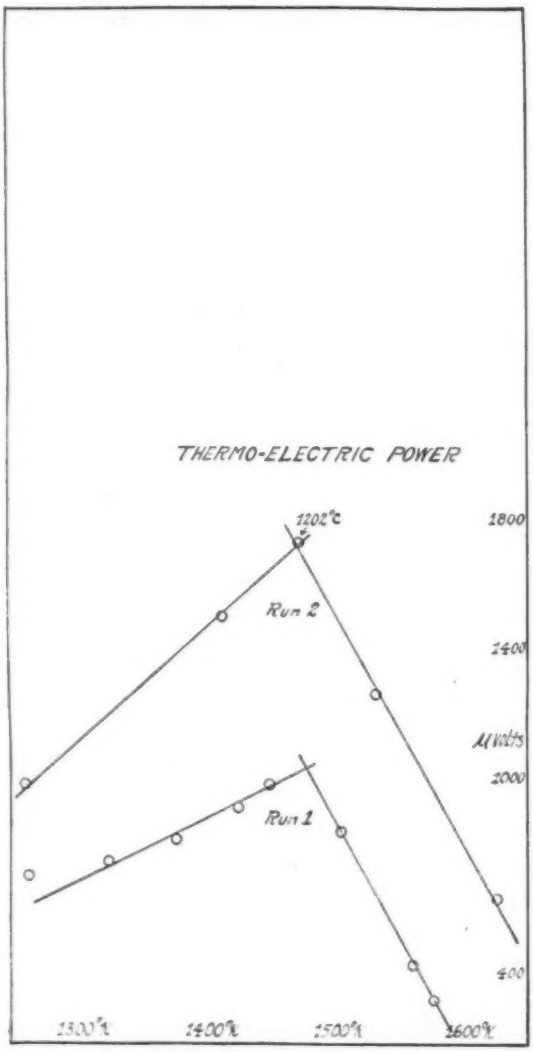

Fig. 4.

Since the equation is satisfied, the conductivity appears, on the basis of the derivation of the equation tested, to be electronic in the 275°C to 750°C range. However, some polarization which occurred in the runs indicates that electrolysis is also involved in the conductivity.

Fig. 2 shows the logarithmic plot for specimen one. Here as in the plot of Eq. (4) a straight line is obtained from 257°C to 750°C with points erratic beyond 750°C.

The plot of $-(1/\rho)(d\rho/dT)$ against $1/T^2$ for a second specimen is shown on Fig. 1. This specimen, baked in a platinum furnace, gave a constant value of resistance for 1500°C after six hours heating. The Eq. (4) in this case is followed for the 1160°C to 1360°C range.

A second run on specimen 2 for a 980°C to 1530°C range gave points that were rather erratic for the test of Eq. (4). Fig. 3 shows the results for this range for log conductivity plotted against $1/T$.

As a check on the break occurring at 1227°C two runs of thermoelectric power plotted against average temperature is shown in Fig. 4. The 1227°C

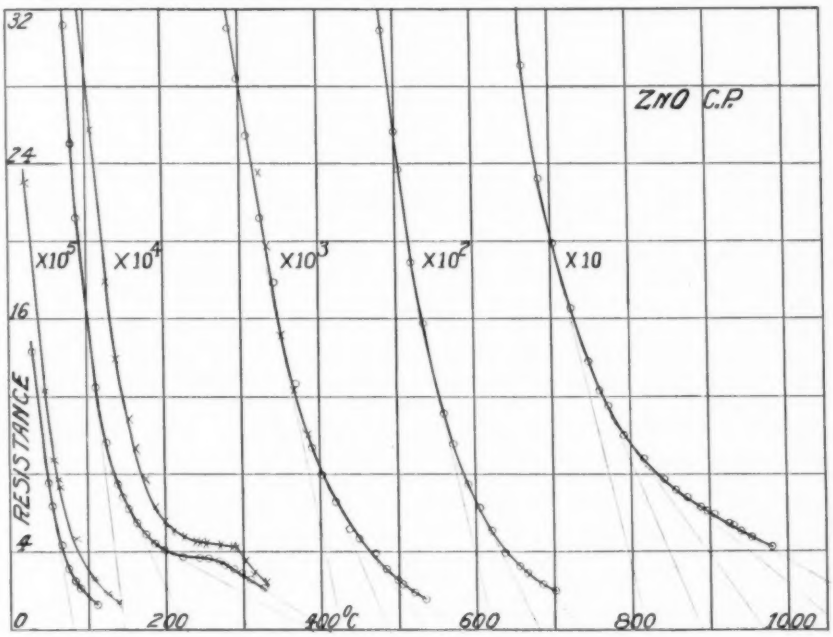

Fig. 5.

break correlates very well with the 1200°C thermoelectric power break.

Fig. 3 also shows the 1160°C to 1360°C run plotted logarithmically.

Discussion of Data for ZnO

Fig. 5 is the third of the resistance-temperature runs for a specimen of C.P. ZnO. The circles indicate the points obtained with decreasing temperature, the crosses with increasing temperature. This partial run from room temperature to about 400°C was made in order to check the peculiar curvature in the 250°C to 300°C range. Each of the three runs showed definitely this peculiarity.

A preliminary run made after the specimen had been baked for thirty minutes in the iron container in which it had been compressed gave quite erratic results in particular throughout the region 550°C to 250°C. The speci-

men was therefore baked for about four hours at approximately 1000°C. After this, runs one, two, and three were made which gave such curves as shown in Fig. 5. The heating interval necessary between runs evidently changed the condition of the specimen since these three curves differed in absolute values of resistance.

From the curves of the three runs tangents were drawn and the data plotted according to Eq. (4), (Fig. 6).

The three plots give straight lines from 550°C to 950°C and from 25°C to 175°C with a transition from 175°C to 550°C. The two lines have different slopes, but the same resistance intercepts. The plots of these runs show that

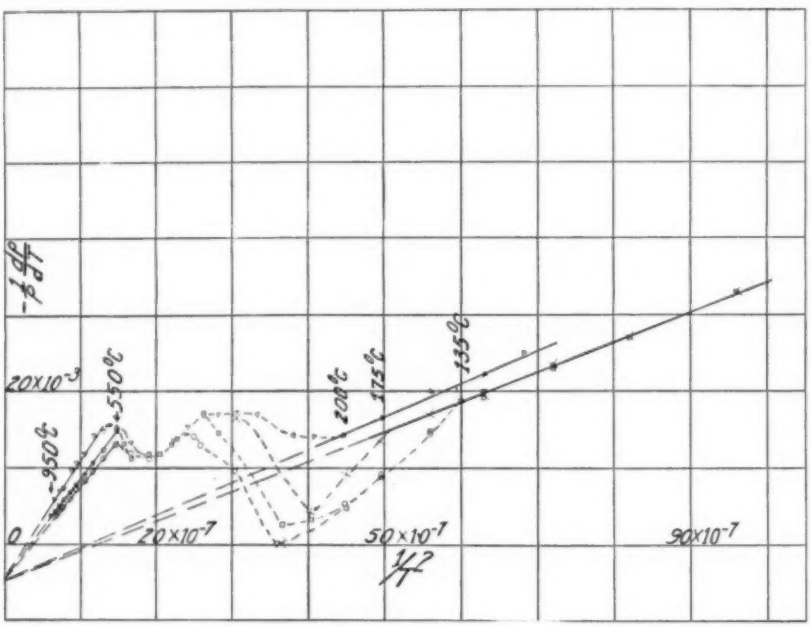

Fig. 6.

with successive heatings to 1050°C there occurs continued decreases in the slope of the line for the 500°C to 1000°C range but no change in the resistance intercept. The line for the 25°C to 175°C range repeated for values of slope and intercept after run one.

On the suggestion of H. M. Cyr of the New Jersey Zinc Company that the transition indicated in the 175°C to 550°C range might be due to impurity, a new sample of S. P. ZnO supplied by the New Jersey Zinc Company was studied.

Fig. 7 shows both the temperature-resistance curve and the plot for

$$[-(1/\rho)(d\rho/dT)] = Q/RT^2 - a.$$

The break in the 250°C to 300°C range does not clearly appear in the temperature-resistance curve as it did in the C.P. specimen. However, the plot of $[-(1/\rho)(d\rho/dT)]$ against $1/T^2$ indicates an irregularity in the 200°C to 550°C range similar to that obtained in the C.P. specimen.

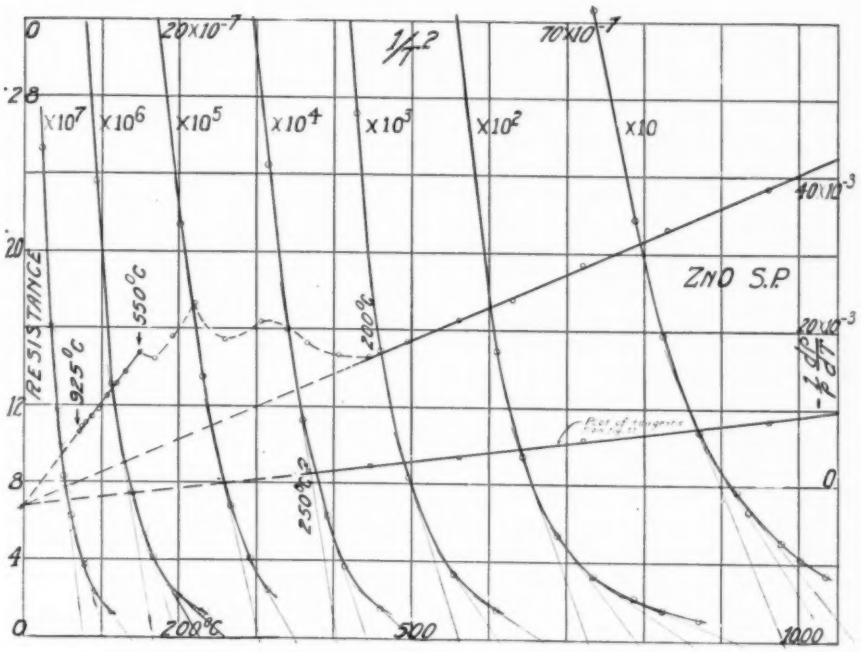
RESISTANCE
ZnO S.P.
x10⁷
x10⁶
x10⁵
x10⁴
x10³
x10²
x10
20x10⁻⁷
70x10⁻⁷
40x10⁻³
20x10⁻³
925°C
550°C
200°C
250°C
208°C
500
1000

Fig. 7.

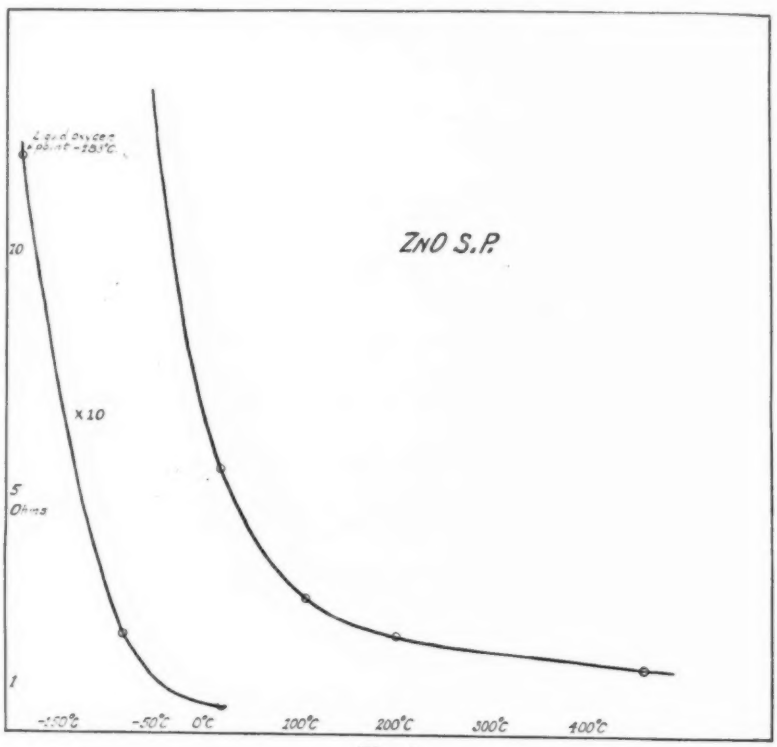
ZnO S.P.
x10
5
Ohms
1
-150°C
-50°C
0°C
100°C
200°C
300°C
400°C

Fig. 8.

This irregularity in the 200°C to 550°C range seems to be related to the growth of particles since below 500°C some change apparently occurs as rubber tests, which are very sensitive to particle-size, show measurable differences if the oxides have been heated to 300°C. There is also an apparent electronic change in this region which is indicated by the yellow color of zinc oxide. Experiments by the New Jersey Zinc Company have shown that at 350°C a yellow tint is just noticeable to the eye. On further heating, the color gradually brightens and becomes a deep pure yellow at 500°C. After

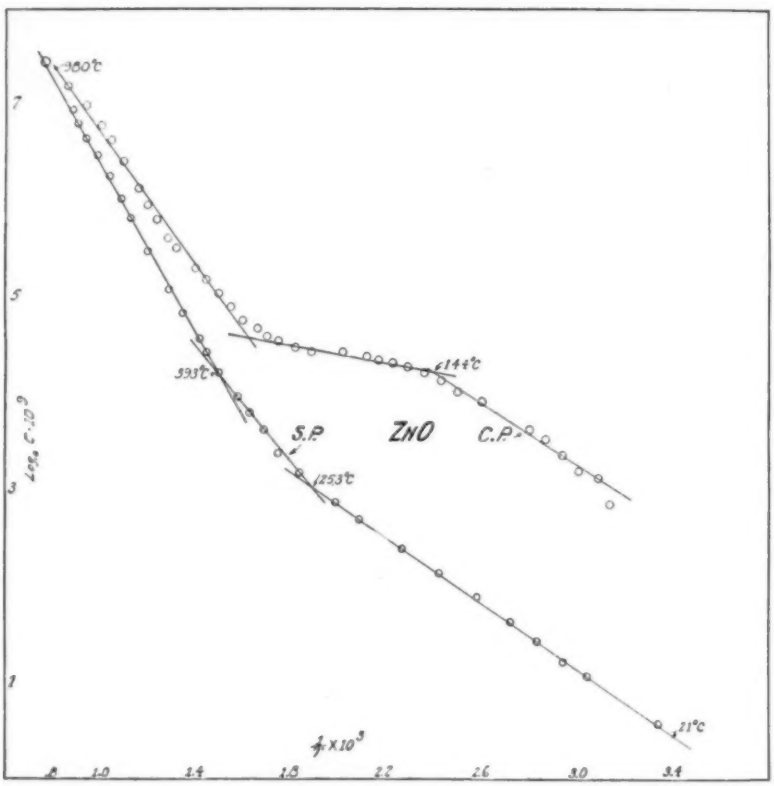

Fig. 9.

500°C a more stable condition is reached as indicated by the fact that Eq. (4) follows a straight line above 550°C.

In connection with the yellow tint mentioned above, it was found that the S.P. ZnO subjected to the 10,000 pounds per square inch pressure became lightly yellow even for room temperature. On heating and then cooling to room temperature the material became white again.

The above runs were made in a nichrome wound furnace. Fig. 8 shows the temperature-resistance run for the S.P. specimen of ZnO when run in a platinum-wound furnace. The temperature about the specimen was raised to approximately 1500°C, where the resistance measured about one ohm. On decreasing the temperature the resistance increased very slowly reaching a value of 1.4 ohms at 470°C. Thereafter the resistance increased rapidly

enough to give the curve of Fig. 8. From this curve tangents were drawn and the plot of $[-(1/\rho)(d\rho/dT)]=Q/RT^2-a$ gave the lower straight line shown in Fig. 7, which has a different slope but same intercept as the 925°C to 550°C and 200°C to 25°C lines.

The specimen during the above run shrank and formed quite noticeable crystals on the surface. The color was green. The specimen also showed the property of rectification. This property is the same as that found by the New Jersey Zinc Company for clinkers of zinc oxide taken from their furnaces and used in earlier radio work for rectifiers.

Fig. 9 is the logarithmic plot for both the C.P. and S.P. specimens. The transitions in these correlate very well with those of the Eq. (4) plot.

The author is indebted to Professor C. C. Bidwell for supervision in this work, and to Mr. H. M. Cyr of the New Jersey Zinc Company for the S.P. zinc oxide.

Flow of Liquids through Porous Media under the Action of Gravity

R. D. WYCKOFF, H. G. BOTSET AND M. MUSKAT
Gulf Research Laboratory, Pittsburgh, Pennsylvania

(Received June 16, 1932)

Recent published results of studies on the flow of liquids through porous media under the action of gravity have shown wide disagreement in both the formulation and interpretation of the problem. A new attack on the problem has been carried out and has led to unambiguous answers to the questions of interest. Experiments on a radial sector of sand show that the old Dupuit formula of 1863 stating that the fluid outflow is proportional to the square of the differences in the fluid heights in the sand is exact within experimental error provided the fluid heights are replaced by fluid heads as measured at the sand bottom. Both the pressure distribution formula and the integrated expression for the fluid outflow are verified in detail. The cases where an added pressure head is superposed upon the gravity flow, heretofore not mentioned in the literature, behaves both with regard to its pressure distribution and fluid outflow as a direct superposition of the simple gravity flow and pure radial flow systems. A semi-quantitative treatment is given for the flow in the capillary zone above the main fluid body. It is necessary under certain experimental conditions to correct for the added flow carried by the capillary layer in addition to that induced by the gravity drive. In most practical cases the capillary flow may be ignored. A theoretical discussion is given of the conditions at the free surface of a gravity flow system and it is shown that nowhere on it can the slope exceed 45°. The results on the radial flow experiments are also generalized to give a method for treating general drives.

I. PURPOSE OF INVESTIGATION AND CRITIQUE OF PREVIOUS INVESTIGATIONS

IT HAS very frequently been assumed that the effect of gravity is an entirely negligible factor in the production of oil from sands. It is true that during the early period of production while the sand pressures are fairly high and the pressure at the well is maintained relatively high, the contribution of gravity flow to the total is negligible or entirely absent. However, when the reservoir is depleted of its gas and the oil has lost its expulsive powers due to depletion of dissolved gases, one cannot arbitrarily ignore the effect of gravity on production rates. To derive a definite answer to this problem was the aim of the following investigation since, as will be seen presently, the results presented in the available literature on the subject can hardly be considered as satisfactory.

Although the problem of gravity flow does not seem to have been considered from the point of view of its relation to oil production it has been given considerable attention by investigators interested in artesian flow and irrigation problems. Nevertheless, a review of the literature shows that neither from an experimental nor from a theoretical point of view has a definite solution to the problem been obtained.

Thus, as long ago as 1863 Dupuit[1] made the assumption that for small inclinations of the free surface the stream lines can be taken as horizontal and

[1] J. Dupuit. Etudes Theoriques et Pratiques sur le Mouvement des Eaux.

are associated with velocities independent of the depth, being equal to that at the free surface (shell flow cf. §6). In particular he derived a formula applying to radial gravity flow. This was then generalized by Forchheimer[2] so as to give a general equation for the free surface of any gravity flow system (cf. §7 Eq. (20)). Although the assumptions underlying these equations have but little validity in regions surrounding the surfaces of outflow of the systems (cf. §6), they have been used indiscriminately by Forchheimer and others in solving special problems, apparently without any attempt to test empirically the predictions they found.

Perhaps the most satisfactory study of any problem of gravity flow in porous media is the elegant treatment by Hopf and Trefftz[3] of the problem of the partial drainage by a ditch of the regional gravity flow in a water sand with an inclined impermeable bed. This problem, idealized as a two-dimensional one, was solved exactly by these authors by using the method of conjugate functions as applied to the rigorously valid Laplace's equation in the interior of the sand (cf. §6). Unfortunately, however, this method cannot be extended to three dimensional cases such as the radial flow problem studied in the present investigation.

Another rigorous attack on the problem of gravity flow, that is, one using solutions of the potential equation (cf. Eq. (13a)), was made even earlier by J. Kozeny[4] with special reference to the case of radial flow. Unfortunately, however, Kozeny neglected entirely the discontinuity between the fluid height in the sand at the well face and the fluid level in the well. Thus he required of his uppermost streamline, which represented the total flux through the system, that it leave the sand body at the fluid level in the well. Further, Kozeny made no attempt to make his uppermost or free surface streamline correspond to a real free surface over which the potential function at any point is directly proportional to the vertical coordinate of that point. Then, too, Kozeny's result that the flow through the system is proportional to the well radius depends on the assumption that the well radius is large as compared to the maximum fluid head in the sand. Just the converse, however, corresponds to most cases of practical interest and when it is taken into account even Kozeny's formulae give an inverse logarithmic variation with the well radius, as is found in the present investigation (cf. §4, Eq. (4)).

It therefore appears that although Kozeny's method of attack is quite rigorous, the assumptions made in its development must necessarily vitiate the validity of his conclusions. Thus it is not surprising that he gets the peculiar result that the flow through a radial flow system is a maximum when the fluid head within the well is half of that at the external boundary. Likewise, Kozeny's result that the flow would vanish with vanishing fluid head in the well is clearly due to the neglect of the discontinuity at the well.

The apparent check of Kozeny's results by Kozeny[5] himself or the more

[2] Ph. Forchheimer, Zeitschr. d. Arch. u. Ing. Ver. Hannover (1886).
[3] Hopf and Trefftz; Zeitschr. f. angew. Math. u. Mech. 1, 290 (1928).
[4] J. Kozeny. Wasserkraft u. Wasserwirtschaft, **22,** 120 (1927).
[5] J. Kozeny. Wasserkraft u. Wasserwirtschaft **22,** 146 (1927).

extensive experiments by R. Ehrenberger,[6] however, do not seem conclusive. Thus the point in Kozeny's empirical data which he takes as the indication of the maximal Q for the fluid well height, being half of that at the back of the sand, might well be taken as being due to experimental error since it cannot lie upon any smooth curve drawn to represent a major part of the data. Since for comparison the Dupuit equation (cf. Eq. (18)) was forced to pass through this point it cannot be expected that it would check with the other points that do lie on a smooth parabolic curve.

Ehrenberger's experiments, though beautifully performed and exhaustive in many respects, do not seem to give a satisfactory answer to the problem. In his desire to correlate his results with Kozeny's theory, Ehrenberger was unfortunately misled in his method of analysis. Thus when he finds that Kozeny's formula does not work he sets up an empirical correction factor which evidently has no physical significance. If he had replotted his Fig. 20 as Q *vs.* ΔZ^2, as suggested by the Dupuit formula and as done in the following discussion, rather than as Q *vs.* Z_w, as suggested by Kozeny's formula, Ehrenberger would have found a straight line confirming the present investigation and would not have had to resort to the empirical correction factor.

It will be clear, therefore, that in spite of the many studies already carried out on the problem of gravity flow in liquids a satisfactory description of the problem had not been attained. The investigation to be described below was undertaken in an attempt to clear up the situation and to derive a conclusive answer with regard to as many features of the problem as possible.

II. Experimental Equipment and Procedure

The principle of the experiments was essentially that of constructing a section of a model well flowing under the action of gravity and observing the production rate under various conditions of flow. It should be mentioned at this time that while the original equipment was designed for gravity flow only, it was found imperative that permeability[7] measurements be made on the sand *in place* in the model, and a second model was therefore constructed. The later model was pressure tight so that from strictly radial flow measurements the actual permeability of the sand could be accurately measured. In addition this model permitted an experimental check on the composite flow formula deduced from a knowledge of the radial and gravity systems.

The initial gravity flow setup was that indicated in Fig. 1. While the same results were obtained from the second and more complete apparatus, a discussion of the former is included because of the more complete data obtained on pressure distributions together with some observations on the behavior of the fluid in the capillary zone.

In Fig. 1, the sector of 15° represents 1/24 of a complete radial flow system. The 152.4 cm length of the sector corresponds to the 152.4 cm closest to a well of radius 5.95 cm which is the distance at which the screen simulat-

[6] R. Ehrenberger; Zeitschr. des Oster. Ing. u. Arch. Ver. Heft 9/10, 11/12, 13/14 (1928).

[7] By the term permeability is meant the fluid outflow through a unit cross section under the action of a unit pressure gradient. It is a constant of the sand and liquid system and inversely proportional to the viscosity of the liquid.

ing the well face was placed. The model was made covering only the immediate neighborhood of the well in order to be able to study in particular the detailed effects of the convergence near the well and the fluid heights in the well, on the free liquid surface within the sand and on production rates. It is clear that at great distances from the well the free liquid surface will be nearly horizontal and the flow will be essentially of a radial horizontal character. This portion, representing the region remote from a well is simulated by the sand-free tank used as a reservoir in the model. Thus except for the height of the sand (40.5 cm), necessarily small in the laboratory, the setup represents closely a full scale model.

The sand reservoir was separated from the sand-free chamber in the back by a fine screen supported against a brass plate perforated uniformly by 1/2″ holes with staggered 5/8″ separations. This insured a uniform distribu-

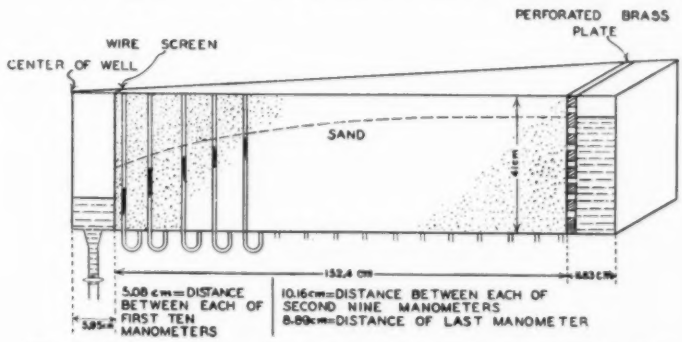
PERFORATED BRASS PLATE
WIRE SCREEN
CENTER OF WELL
SAND
132.4 cm
5.08 cm = DISTANCE BETWEEN EACH OF FIRST TEN MANOMETERS
10.16 cm = DISTANCE BETWEEN EACH OF SECOND NINE MANOMETERS
8.89 cm = DISTANCE OF LAST MANOMETER

Fig. 1. Diagram of apparatus for radial gravity flow experiments.

tion of liquid against the far end of the sector. The sand-free tank continued 12 cm beyond the screen and plate. The glass sides were sealed to the brass frame with beeswax-rosin mixture. The sand used was a fairly uniform Ottawa sand of about 30/inch mesh. From the preliminary tests with an earlier setup it was learned that unless special precautions were taken in filling the sector with the sand and water, air bubbles would be trapped in the sand pores and destroy the homogeneity of the pore openings for the flow of the liquid. The procedure finally adopted in filling the sector was that of thoroughly mixing and stirring the sand by hand while keeping the water level in the tank just above the sand. Each layer of sand was freed of air before more was added. From the uniformity of appearance of the sand as seen through the glass sides one could tell if the sand were really free of trapped air.

From holes in the bottom of the sector placed along the central radius, twenty small manometer tubes were led and mounted next to one of the glass sides at points corresponding to their entries in the bottom. The ten tubes nearest the well were placed at one half the separations of those nearer the far end since the pressure gradients change most rapidly near the well and it is here that the greatest detail was desired. These tubes, of course, indicate hydrostatic pressures at the bottom of the sand. It was hoped, and in fact turned out to be true, that these *effective pressures* are all that are required to predict completely the production from the well.

The outlet from the bottom of the well was furnished with a stop-cock so as to control the height of fluid in the well and hence the production rate. A pump was connected to the outlet collecting vessel to pump the outflow water back into the inflow tank, thus maintaining a steady condition of flow for given levels in the tank and well. This circulation eliminated the accumulation of air bubbles in the sand which would occur if fresh water were continually supplied to the system.

The experiments consisted essentially in noting the rate of outflow of water from the sand for given heights of the water level in the tank at the back of the sector and in the well at the apex. Readings were also taken of the heights in the various intermediate manometer tubes. The experiments

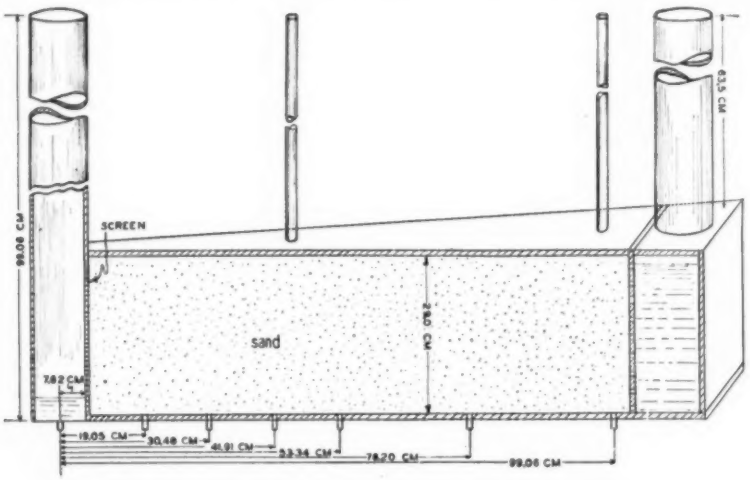

Fig. 2. Diagram of apparatus for composite (radial drive plus gravity) flow experiments.

were so conducted that the water level was never appreciably raised into an upper zone containing air. This precaution was to confine the flow to air-free sand and when it was necessary to increase fluid heights the tank was emptied of sand and properly refilled.

While good use was made of the pressure distributions obtained from this setup it was found impossible to obtain *effective permeability* values for use in computing output volumes. It was therefore necessary to construct a new pressure tight flow tank in which permeability tests could be made on the sand in place. Before going into further detail as to experimental results we will describe briefly the second setup used in the final production rate tests and in the work on composite flow.

The general arrangement of the second flow tank is shown in Fig. 2. This was again a 15° sector with a well screen at the apex and a sand-free tank section at the back end. The entire sector was constructed of 6.3 mm brass plate reinforced with angles to prevent flexure of the sides. All joints were soldered except the top plate which was screwed to the top flanges with a rubber gasket interposed. Each end of the flow tank was equipped with a stand pipe

some 10 cm in diameter and extending 65 cm above the top of the sand sector thus enabling the system to be operated as a purely radial flow system by maintaining the fluid level at the apex or well end, above the sand level. Obviously it was necessary to close in the top of the sand body, and to make certain that no free space existed between the top of the sand body and the top plate of the tank, three glass standpipes 2.5 cm diameter and 65 cm long were cemented into the top plate to serve as sand reservoirs. After carefully packing the sector with sand as previously described until completely filled, the upper plate was bolted in place with a rubber gasket to seal the flange. Water was then circulated continuously with levels at both ends held above the sand height. Continuous jarring of the tank served to settle the sand and additional sand to fill any voids created, was fed into the sector from the sand reservoirs. This process was continued until the permeability reached a minimum value under radial flow tests. This minimum permeability was also checked against the value obtained in a simple glass tube linear-flow apparatus where careful packing and elimination of sand-free spaces may be observed visually. By this means we were certain that no sand-free channels existed in the sector. Preliminary experiments showed the absolute necessity of this rather elaborate procedure.

In addition to manometers for measuring the fluid head at the entrance and well ends of the sector, five additional manometers were provided to measure intermediate pressures. A variable speed gear-pump was used to circulate the water continuously at any desired rate and a carefully calibrated orifice-plate flow meter was used to measure flow rates. By this means absolutely steady state flow conditions could be maintained.

As before, the experiments consisted in observing flow rates as a function of pressure differentials maintained between the boundaries of the flow system with intermediate pressure readings as a further check. The tests included purely radial flows for effective permeability determinations; flows in which the input water level was held above that of the sand, while at the well end the fluid level was below the sand height, that is, the composite flow case; and the usual gravity flow test in which the fluid levels at the both ends were below sand height. In order to eliminate the effect of air bubbles the same precautions mentioned above were observed, that is, fluid levels in the sand were never raised into an upper zone containing air, all changes in water level being made downward.

III. Qualitative Discussion of Results

Pressure distribution and flow rate data

The results of the observations from one set of experiments with the sector of Fig. 1 are given in Table I. These data give the pressure distribution for various liquid heights in the well and the resultant production rates. A similar set of observations is given in Table II, the difference being that in the latter set the fluid height at the input end of the sector was varied through a considerable range. The purpose of showing both sets of data is to show the effect of flow in the capillary layer, a feature which will be brought out later on.

TABLE I. *Flow tank of Fig. 1.*

Gauge No.	Run No. 1 Pressure head (cm)	Run No. 2	Run No. 3	Run No. 4	Run No. 5	Run No. 6	Run No. 7	Run No. 8	Run No. 9	Run No. 10
Well	29.10	27.85	23.30	20.20	15.10	10.90	10.60	6.10	0	0
1	29.45	28.15	24.30	21.80	17.70	14.70	14.40	11.80	9.90	10.15
2	29.60	28.40	25.25	23.30	20.20	18.00	17.70	16.00	15.05	15.00
3	29.75	28.55	25.85	24.30	21.80	20.10	19.75	18.50	17.80	17.50
4	29.90	28.65	26.35	25.00	22.90	21.50	21.15	20.10	19.45	19.15
5	30.10	28.85	26.85	25.70	23.90	22.80	22.35	21.45	20.90	20.55
6	30.10	28.85	27.10	26.20	24.70	23.75	23.25	22.45	21.95	21.50
7	30.25	29.00	27.50	26.70	25.40	24.65	24.15	23.40	22.95	22.50
8	30.35	29.20	27.95	27.20	26.15	25.45	24.95	24.30	23.90	23.40
9	30.50	29.20	28.10	27.50	26.60	26.00	25.50	24.85	24.50	23.95
10	30.45	29.20	28.20	27.70	26.90	26.40	25.85	25.25	25.00	24.35
11	30.45	29.20	28.50	28.15	27.55	27.20	26.60	26.10	25.75	25.20
12	30.60	29.30	28.80	28.60	28.10	27.85	27.20	25.75	26.50	25.85
13	30.60	29.40	29.00	28.90	28.55	28.40	27.70	27.35	27.05	26.40
14	30.70	29.45	29.20	29.20	29.00	28.90	28.20	27.85	27.60	26.90
15	30.80	29.55	29.50	29.50	29.40	29.30	28.65	28.40	28.10	27.45
16	30.90	29.70	29.75	29.85	29.85	29.90	29.20	28.90	28.65	27.95
17	30.90	29.70	29.85	30.00	30.10	30.20	29.45	29.20	28.90	28.25
18	30.90	29.65	29.95	30.15	30.35	30.45	29.75	29.55	29.35	28.60
19	30.95	29.70	30.10	30.30	30.60	30.65	30.00	29.85	29.70	28.90
20	31.05	29.75	30.25	30.55	30.90	31.00	30.40	30.25	30.10	29.30
Rate cc/sec.	2.75	2.68	9.05	13.15	18.12	21.60	21.60	22.30	22.70	21.3

In the second set of experiments the top free surface of the liquid in the sand was also noted as accurately as possible and recorded. Two sets of these readings which are typical of all these sand height data are plotted in Fig. 3.

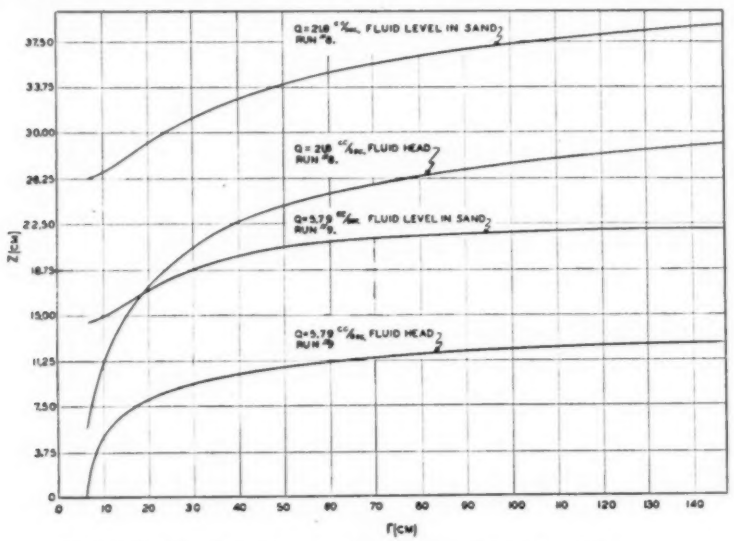

Fig. 3. Fluid levels and fluid heads in sand (gravity flow).

Details of flow—streamlines and capillary flow

As will be seen later, the data already given are sufficient to give a descrip-

TABLE II. *Flow tank of Fig. 1.*

Gauge No.	Run No. 11 Pressure head (cm)	Run No. 12	Run No. 13	Run No. 14	Run No. 15	Run No. 16	Run No. 17	Run No. 18	Run No. 19
Well	32.50	27.70	22.50	17.00	16.00	15.60	7.00	5.80	0
1	33.50	29.30	25.00	20.60	19.40	18.20	12.50	11.30	5.80
2	34.20	30.50	26.90	23.40	22.00	20.20	16.20	15.10	7.30
3	34.80	31.70	28.40	25.80	24.10	21.80	18.80	17.60	8.30
4	35.30	32.60	29.80	27.50	25.70	23.10	20.70	19.40	8.90
5	35.85	33.40	31.00	29.00	27.00	24.10	22.30	20.80	9.50
6	36.20	34.00	31.90	30.10	28.00	25.00	23.30	22.00	9.90
7	36.60	34.60	32.70	31.10	28.90	25.70	24.30	22.80	10.30
8	36.80	34.90	33.20	31.70	29.60	26.20	25.10	23.60	10.60
9	37.00	35.40	33.90	32.50	30.20	26.60	25.80	24.10	10.90
10	37.20	35.60	34.20	33.00	30.50	26.90	26.10	24.40	10.90
11	37.60	36.30	35.00	34.10	31.50	27.60	27.10	25.40	11.20
12	37.80	36.70	35.60	34.80	32.20	28.10	27.80	26.10	11.60
13	38.10	37.10	36.20	35.50	32.70	28.60	28.30	26.60	11.70
14	38.30	37.50	36.70	36.10	33.20	29.00	28.90	27.10	11.90
15	38.40	37.80	37.20	36.80	34.00	29.60	29.60	27.80	12.30
16	38.70	38.10	37.50	37.20	34.40	29.80	29.90	28.00	12.40
17	39.10	38.70	38.20	38.00	34.90	30.30	30.50	28.60	12.70
18	39.10	38.80	38.50	38.30	35.10	30.40	30.80	28.80	12.70
19	39.30	39.10	38.80	38.70	35.50	30.60	31.00	29.20	12.90
20	39.30	39.30	39.10	39.00	35.90	31.00	31.50	29.50	13.10
Rate cc/sec.	10.70	17.10	22.90	28.10	24.30	18.00	23.90	21.80	5.79

Radius—apex of system to gauge $(n) = r_n$

	cm		cm		cm		cm
r_w	6.4	r_5	30.5	r_{11}	66.0	r_{16}	116.8
r_1	10.2	r_6	35.6	r_{12}	76.2	r_{17}	127.0
r_2	15.3	r_7	40.6	r_{13}	86.4	r_{18}	137.2
r_3	20.3	r_8	45.7	r_{14}	96.5	r_{19}	147.3
r_4	25.4	r_9	50.8	r_{15}	106.7	r_{20}	156.0
		r_{10}	55.8				

tion of the problem as a whole. Some interesting information as to the details of the flow in the sand was obtained in the following manner. A narrow tube with a capillary opening at the tip was forced down vertically into the sand at the glass face and near the back end of the sector. Small quantities of black ink were added through this tube so as to maintain a small steady flow of ink from the tip into the sand. This ink formed streamers that progressed along the sector towards the well with surprising sharpness. They clearly proved that the flow in the sand was of a streamline character and at the same time they traced out these streamlines.

The detailed positions of these streamlines were recorded and then plotted. The results are shown in Fig. 4. The minor irregularities are undoubtedly due to local inhomogeneities in the sand body. The downward slope of the lower streamlines at the tank end may be explained by the fact that the lowest row of holes in the back plate was about 1 cm or more above the bottom so that water entering the sand from the supply reservoir must diverge downward as indicated by the streamlines in this region.

Of more interest are the marked upward slopes of the upper streamlines at the reservoir end of the sector. This may at first seem surprising since one might at first suppose that the upper part of the wetted sand would be a *dead* capillary layer taking no appreciable part in the flow. When it is recalled however that due to the pressure discontinuity across the capillary free surface there must be a pressure deficiency immediately below it, it becomes clear that the capillary layer instead of being dead should actually act like a syphon and play a significant part in the flow of the liquid. To do so obviously requires that upon entering the sand-body from the supply tank, the streamlines in and near the capillary layer slope upwards as was observed. Further discussion as to the amount of the flow occurring in the capillary zone will be presented later.

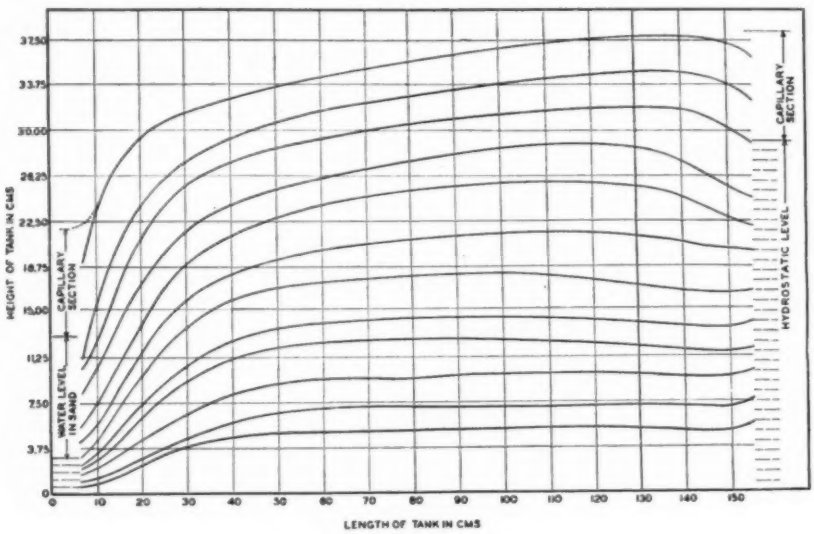

Fig. 4. Observed streamlines.

Besides the character of the streamlines near the tank it is of interest to note their nature near the well. Although the data are not sufficiently accurate to yield exact values of the slopes of the streamlines it is fairly clear from the curves that only the very upper ones have inclinations with the horizontal exceeding 45°. Further, it is to be noted that the capillary free surface itself is much flatter near the well than the streamlines below it and in fact goes through an inflexion as is indicated more clearly in Fig. 3. These qualitative features fit in directly with some analytical results to be given in §6. There it is shown that under no conditions in gravity flow in a homogeneous medium (neglecting kinetic energy) can the slope of a *free* surface exceed the value 1, corresponding to an inclination of 45°. In general, the slope of an ordinary streamline will have an upper limit lower than 1. Only if the pressure distribution is such that the vertical velocity decreases with the height may one get inclinations exceeding 45°. Since there is a pressure deficiency underneath the capillary free surface it is quite possible that as one

goes into the capillary layer the effect of the capillary surface will be to decrease the vertical velocities and thus make the slopes exceed 1. Hence the inclinations exceeding 45° are even to be expected for such streamlines. Further, since the capillary surface itself cannot exceed 45° the streamlines immediately below it, near the well, should break away and leave a space relatively dead in the immediate neighborhood of the well and just below the free capillary surface. This too, corresponds to the observations as is indicated by the slope of the free surface right at the well (cf. Fig. 3).

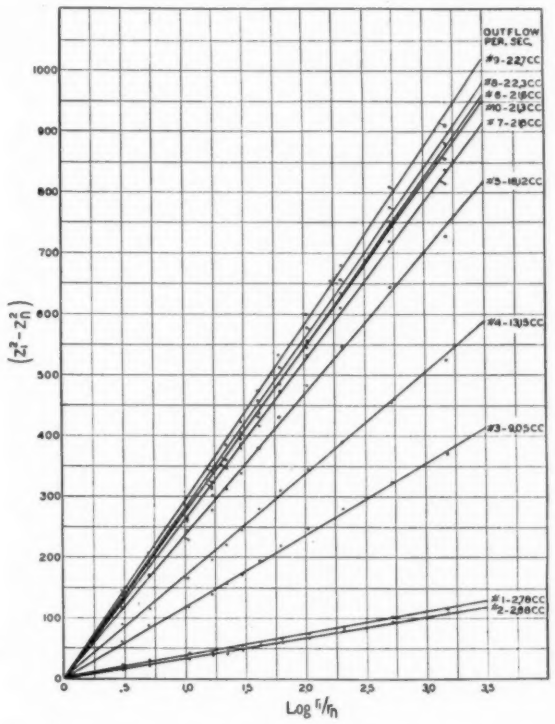

Fig. 5. Relation between fluid head and distance from outer sand face for various rates of flow.

IV. The Quantitative Results

Pressure distribution

For purposes of application a quantitative formulation of the results of the investigation must be developed. From theoretical considerations it appears that the phenomena should be described by an equation for the free liquid surface involving as parameters, the heights in the tank and well or the production rate from the system. Such a development is in fact outlined in §6. It will be found, however, that in attempting a rigorous analytical solution, it is impossible to carry through in detail a satisfactory treatment of the problem. Our procedure therefore has been that of analyzing the experimental data to obtain an empirical formulation of the result.

As the most accurate data of the experiments were the readings on the manometer tubes, these were plotted to see if they implied any definite empirical relation. In Fig. 5 is plotted $Z_1^2-Z_n^2$ against $\log_e r_1/r_n$ for fixed values of the production Q. Z_1 is the fluid height in the manometer tube farthest from the well at radius r_1 and Z_n is the manometer reading at radius r_n taken at each of the points along the sector at which a manometer was attached. The production rate obtained for the pressure conditions represented by each curve is shown. The curves plotted in Fig. 5 are calculated from the experimental data of Table I. It will be noted that within experimental error the curves are linear and pass through the origin.

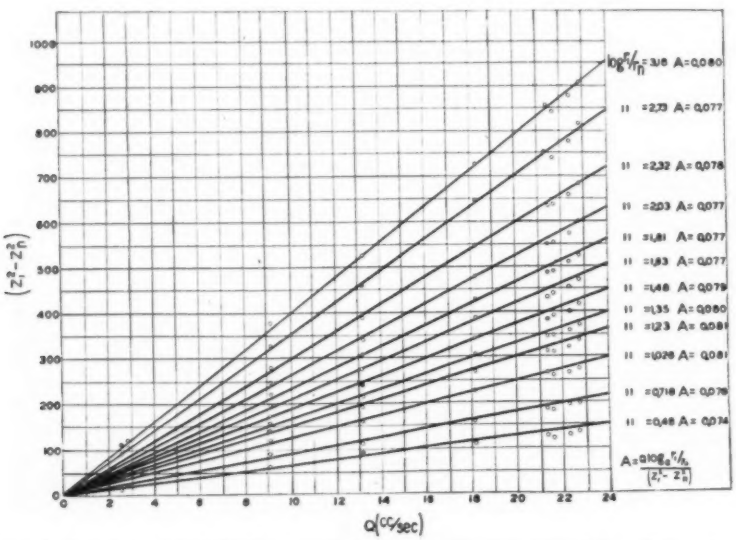

Fig. 6. Relation between fluid head and distance from outer sand face for various rates of flow for determination of the constant A.

In Fig. 6, the same data are plotted with ordinates $Z_1^2-Z_n^2$ against the production rate Q for fixed values of $\log r_1/r_n$. It will again be seen that the curves are linear and pass through the origin.[8] It follows at once that the following relation must hold between $(Z_1^2-Z_n^2)$, Q, and $\log r_1/r_n$

$$A(Z_1^2 - Z_n^2) = Q \log_e r_1/r_n \qquad (1)$$

where: Z_1, Z_n are the fluid heads at the bottom of the sand at the points r_1, r_n respectively, and A is a constant. The value of the constant A for the twelve different sections of the sector represented by the various points r_n, and at ten different production rates, is shown (Fig. 6) to average 0.078, with an average deviation from the mean within experimental error. This shows the validity of Eq. (1), and there remains the interpretation of the constant A in terms of known constants of the flow system. This determination of A could not be made accurately in these tests because of uncertainty

[8] The discrepancies occurring for large values of Q will be shown later to be due to the effect of the capillary layer.

in obtaining the sand permeability and the unknown capillary effect and was therefore left for an additional experiment with the apparatus of Fig. 2 which will now be considered.

Determination of the flow constant, A

It will be seen from theoretical considerations which will be presented in §6 that in Eq. (1):

$$A = \pi k \gamma g. \tag{2}$$

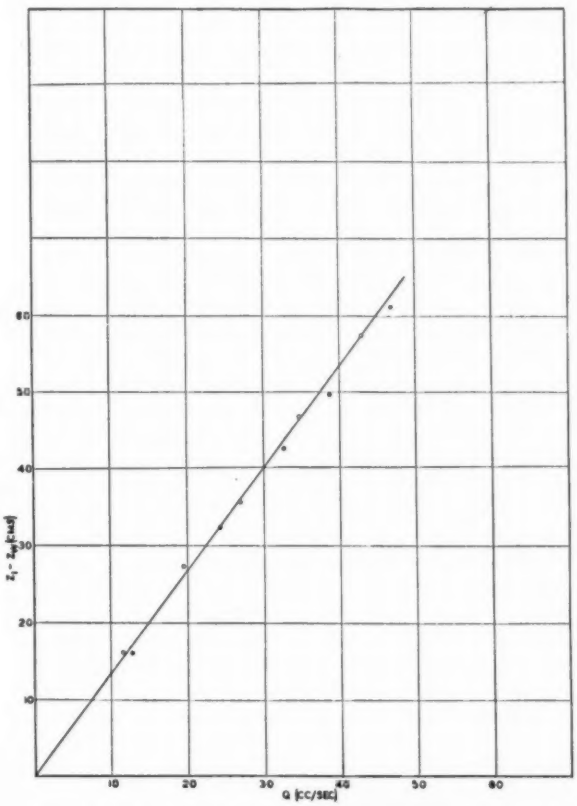

Fig. 7. Permeability determination, pure radial flow. Permeability $k = 264$ cc/sec./cm²/atmos./cm at 20°C.

Considering the neglect of vertical velocities in the theoretical derivation we may reasonably expect, however, that the actually observed value of A will differ from $\pi k \gamma g$ by some appreciable amount which may be determined experimentally.

Experimental data regarding the factor A obtained with the apparatus of Fig. 2 with the procedure which has already been described, will therefore be presented.

Since the only unknown factor appearing in Eq. (2) is the permeability k of the sand, the first step is to determine its value. As mentioned in the description of Fig. 2, this apparatus was suitable for observing flow rates under

pure radial flow conditions, that is, with the fluid levels at the input and output ends of the sector held above the sand height.

Now the outflow from such a system is given rigorously (since the pressure has the role of a velocity potential) by the equation:

$$Q = [2\pi k\gamma g Z_s(Z_1 - Z_w)]/\log_e r_1/r_w \qquad (3)$$

where: Z_s = sand height in cm; Z_1, Z_w = fluid heights at input radius r_1 and well radius r_w respectively. The value of k for the sand in place is therefore readily obtained. Fig. 7 shows the results of two different series of radial flows represented by the circles and dots respectively from which we obtain the value of:

$$k = 264 \text{ cc/sec./cm}^2\text{/atmos./cm}.$$

A gravity flow was next observed holding the fluid level at the input end just below the sand height in order to eliminate as far as possible the capillary flow contribution. The pressure distribution and the rate of flow obtained are shown in Table III.

TABLE III. *Gravity flow. (Apparatus of Fig. 2.)*

	Z_1 (cm)	Z_2	Z_3	Z_4	Z_5	Z_6	Z_w	Q cc/sec.
	28.57	27.47	26.07	25.07	24.07	22.37	18.07	6.61
r (cm)	39.0	30.0	21.0	16.5	12.0	7.5	3.0	
	Sand height = 29 cm							

Applying the above data to the empirical relation previously obtained:

$$A(Z_1^2 - Z_n^2) = Q \log_e r_1/r_n \quad [\text{cf. Eq. (1)}]$$

we obtain the following values for A, considering several values of r_1/r_n:

$$\log_e r_1/r_w = 2.56 \quad A_1 = 0.0346$$
$$\log_e r_1/r_6 = 1.65 \quad A_2 = 0.0345$$
$$\log_e r_1/r_5 = 1.18 \quad A_3 = 0.0329$$
$$\log_e r_1/r_4 = 0.862 \quad A_4 = 0.0305$$
$$A = 0.0331 \text{ average observed.}$$

It has been suggested that we might expect A to be given by $\pi k\gamma g$ modified by some additional factor. In fact, however, applying the value of the sand permeability $k = 264$ cc/sec. determined experimentally (Fig. 7) and putting $\gamma = 1.0$, $g \leqq 0.00097$ atmosphere-cm/density and considering a 15° sector:

$$A = (\pi \times 264 \times 1.0 \times 0.00097)/24 = 0.0335$$

which is in closer agreement with the observed value than would be anticipated, considering experimental error. We are therefore justified in assuming that the factor $\pi k\gamma g$ is exact.

The empirical gravity flow formula (1) may now be written

$$Q = \pi k\gamma g(Z_1^2 - Z^2)/\log_e r_1/r \qquad (4)$$

where: γ = density of fluid, k = sand permeability (cc/sec./cm²/atmos./cm) Z_1, Z are fluid *heads* in cm at r_1 and r respectively, g = acceleration of gravity = 0.00097 atmos.-cm per unit density, Q = fluid flow (cc/sec.).

It is interesting to note that in form this formula is exactly that derived by neglecting vertical velocities.

V. Composite Radial and Gravity Flow

Analysis

It is of practical interest to extend the discussion to include the case in which the fluid level at the input end of the system is greater than the sand height. Such a system corresponds to a gravity flow system in which the input fluid level is at the sand height with a superposed pressure at the outer boundary. Consideration of this composite flow system will suggest that analytically it may be treated as a purely radial flow and a gravity flow superposed.

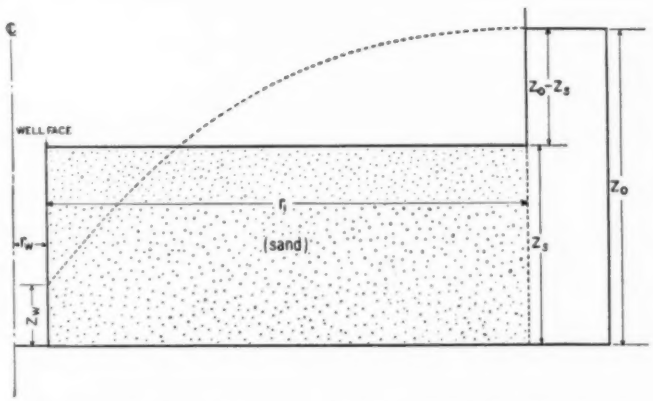

Fig. 8. Diagrammatic representation of composite flow system.

Fig. 8 shows diagrammatically the conditions assumed. Z_0 is the total fluid head at the outer boundary and Z_w is the fluid head at the well. Z_s is the sand thickness. The radial flow component is expressed as:

$$Q_r = 2\pi k\gamma g Z_s(Z_0 - Z_s)/\log_e r_1/r_w. \tag{5}$$

The gravity flow component will be:

$$Q_g = \pi k\gamma g(Z_s^2 - Z_w^2)/\log_e r_1/r_w. \tag{6}$$

The resultant composite flow will be the sum of the above components and is

$$Q_{g,r} = \pi k\gamma g(2Z_sZ_0 - Z_s^2 - Z_w^2)/\log_e r_1/r_w \tag{7}$$

where: Z_0 = total fluid head in cm expressed in terms of the fluid flowing in the sand, Z_s = sand height (cm), Z_w = fluid head at well (cm), r_1 = outer radius (cm), r_w = well radius (cm).

It is also of interest to obtain the equation showing the fluid head distribution in the composite flow system. Again assuming a superposition of

the two types of flow, we readily obtain the expression

$$Z = \frac{(Z_0 - Z_s)}{\log_e r_1/r_w} \log_e r/r_w + \left(Z_s^2 - \frac{(Z_s^2 - Z_w^2)}{\log_e r_1/r_w} \log_e r_1/r, \right)^{1/2} \qquad (8)$$

where Z = hydrostatic head at radius r.

Experimental verification

To test the pressure distribution indicated by the above analysis, Eq. (8), the apparatus of Fig. 1 having 20 manometers was selected as best suited for this purpose. The apparatus was modified by adding a tank extending above the sand level at the input end, thus permitting the water level at this end to be held above the sand level. In addition, after filling the sector with sand and water a layer of plaster of paris about 2 inches thick was poured over the sand top. This effectively sealed the top sand face for moderate pressure

Table IV shows the comparison between calculated and observed fluid heads Z, and shows that, as far as pressure distribution is concerned, Eq. (8) represents the observed facts:

TABLE IV.

r (cm)	Z (calculated) (cm)	Z (observed) (cm)	r (cm)	Z (calculated) (cm)	Z (observed) (cm)
6.4	0	0	55.8	39.9	40.0
10.2	16.4	15.7	66.0	41.8	41.7
15.3	23.5	22.8	76.2	43.0	43.1
20.3	27.8	27.4	86.4	44.4	44.3
25.4	30.6	30.6	96.5	45.6	45.4
30.5	33.0	33.2	106.7	46.7	46.5
35.6	34.9	35.1	116.8	47.6	47.4
40.6	36.5	36.8	127.0	48.3	48.5
45.7	37.6	38.0	137.2	49.1	49.3
50.8	39.0	38.9	147.3	49.7	50.0
			156.0	50.4	50.4

Where the boundary conditions were:

$$Z_0 = 50.4 \text{ cm}, \quad r_1 = 6.4 \text{ cm},$$

$$Z_s = 40.5 \text{ cm}, \quad r_2 = 156.0 \text{ cm},$$

$$Z_w = 0.0 \text{ cm}, \quad Q = 50 \text{ cc/sec}.$$

Verification of Eq. (7) expressing the flow rates is not obtainable from the experiment just cited because no independent value of the sand permeability k was obtainable. However, a new series of tests with the apparatus of Fig. 2 with known sand permeability (Fig. 7) were made for this purpose. The essential observed data and the calculated Q's are given in Table V.

TABLE V. *Composite radial flow.*

Z_0	Z_w	Calculated Q (cc/sec.)	Observed Q	% error
89.47	27.47	46.97	46.1	+1.9
78.38	27.47	38.56	38.4	+0.4
59.67	27.47	24.38	23.7	+2.9
39.37	27.47	8.99	8.6	+4.5
70.87	22.57	36.07	36.1	−0.1
47.57	22.57	18.41	18.5	−0.5
78.37	17.17	44.56	44.2	+0.8
58.47	17.17	29.48	29.0	+1.7
44.97	17.17	19.25	19.3	−0.3
74.37	12.57	43.32	43.5	−0.4
59.57	12.57	32.09	31.5	+1.9
48.17	12.57	23.46	23.9	−1.8
68.17	6.97	40.05	40.8	−1.8
50.87	6.97	26.94	27.0	−0.2
35.55	6.97	15.32	16.4	−6.6
61.47	0.17	35.61	36.1	−1.4
56.47	0.17	31.82	32.1	−0.9
48.17	0.17	25.52	26.7	−4.4
			Average error =	−0.2%

Where: $Z_s = 29.0$ cm, $\pi k\gamma g/24 = 0.0335$, $r_1 = 39$ cm, $r_w = 3$ cm.

These data amply justify the conclusion that the composite flow formula, Eq. (7), gives accurate quantitative results and that considering either the pressure distribution within the system or the quantity output, this type of flow may be resolved into two discrete types; pure radial drive and gravity flow. In any practical application it is obvious that the superposed head imposed at the outer boundary must be expressed as a fluid head in terms of the fluid flowing through the system.

An approximate calculation of the capillary flow

It has been mentioned that flow occurs in the capillary zone (see Fig. 4) and that the experiments from which the flow laws could be derived were necessarily conducted so that the contribution of the flow in this capillary layer was small compared with the total flow. Unless such precautions are taken the capillary flow will not be a negligible factor in the flow system. Thus in Fig. 3, flow No. 9, the capillary zone of 9.5 cm height is practically equal to the fluid head and as a result its contribution is by no means negligible, but is approximately 65 percent of the pure gravity flow. This is an extreme case but if calculations are made for other runs from the data given in Table II it will be found that there is a progressive increase in the discrepancy due to the increased proportion of capillary flow. It is therefore of some interest to obtain an approximately quantitative estimate of the flow occurring in this zone. In most practical cases this detail could be neglected but in many cases, and particularly in experimental work where the capillary rise cannot be made small without incurring serious deviations from pure viscous flow, an approximate calculation is of value.

In Fig. 3 are plotted the fluid head distribution and the corresponding observed fluid levels in the sand for two sets of flow experiments. It should be

mentioned that the fluid heights in the sand cannot be obtained with any great accuracy even though a steady-state flow is maintained for several hours. However, these curves, which are typical of all of a large number of observations, show clearly the capillary layer and the discontinuity which exists between the fluid levels in the well and in the sand face adjacent to the well.

No attempt is made here to study the details concerning this discontinuity. Qualitatively, it is easy to see that vertical velocities must exist in the gravity flow system and that these vertical velocity components give rise to resistance forces in any vertical column which are proportional to the integrated vertical velocities in the column. Thus in Fig. 9 the actual fluid height Z_s in the sand at any point, *neglecting capillarity*, is the observed fluid head Z, (measured at the bottom of the sand) $+\bar{v}Z_s/k\gamma g$, where $\bar{v}$ is the average vertical velocity of the fluid in the column. Unfortunately we do not know the velocity distribution in the system and hence cannot evaluate $\bar{v}\,Z_s/k\gamma g$

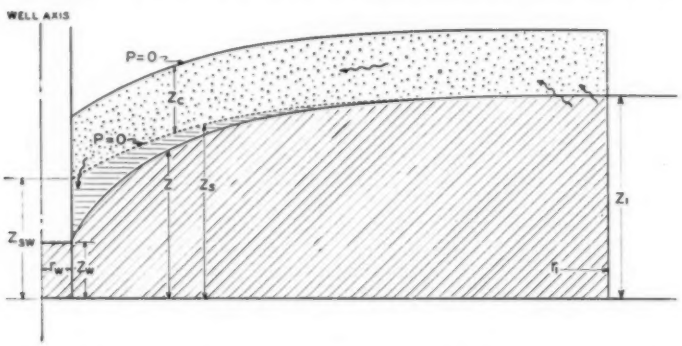

Fig. 9. Diagrammatic representation of gravity flow system showing effect of capillary layer.

which is the difference between fluid heads and fluid heights, existing everywhere in the system. It is obvious, however, that as the fluid level in the well is lowered the vertical velocities increase and the discontinuity $\Delta Z_s = (Z_{sw} - Z_w)$ between the fluid level in the well and in the adjacent sand face, for example, continuously increases. A rough analysis indicates that we might expect ΔZ_s, in the sand, to be at least approximately $\Delta Z/2$ and the data of Fig. 3, together with other observations not shown, confirm this within the accuracy of experimental observations. Assuming that the fluid height in the sand is given by this relation we may proceed with the consideration of the capillary flow.

Fig. 9 shows *schematically* an approximation to the actual flow system where Z_1 and Z_w are the observed fluid heads at r_1 and r_w respectively, Z_1 and Z_{sw} are the fluid heights in the sand, and Z_c is the thickness of the capillary zone. The surfaces indicated as $P=0$ are constant pressure surfaces.

As already mentioned, we may expect the capillary zone to act like a radial flow syphon operating under a differential head

$$(Z_1 - Z_{sw}) = (Z_1 - Z_w)/2.$$

Hence the radial flow in the capillary zone, neglecting end effects which are partially compensating, and assuming the capillary zone to be complete over the entire system, is

$$Q_c = [2\pi k\gamma g Z_c(Z_1 - Z_w)/2]/\log_e r_1/r_w. \tag{9}$$

The purely gravity flow is:

$$Q_g = \pi k\gamma g(Z_1^2 - Z_w^2)/\log_e r_1/r_w. \tag{10}$$

Hence the resultant flow is the sum of (9) and (10), or

$$Q_{g+c} = \pi k\gamma g(Z_1 - Z_w)(Z_1 + Z_w + Z_c)/\log_e r_1/r_w. \tag{11}$$

While this equation cannot be exact it should at least provide an approximate correction for the capillary flow and through its use we will present additional experimental data on gravity flow which gives further support to the validity of the empirical Eqs. (4), (7), and (8).

The data of Table VI cover observations on gravity flow using the apparatus of Fig. 2. The input and well fluid heads are given together with the associated production rates and the calculated values of production using the simple gravity flow formula, Eq. (10), and the calculated production corrected for a complete capillary zone (Eq. (11)), where: $\pi k\gamma g = 0.0335$ (measured—Fig. 10). $Z_c = 9.5$ cm., $\log_e r_1/r_w = 2.56$.

TABLE VI.

Run No.	Z_1	Z_w	Z_s	Calc. Q cc/sec. Eq. (10)	Calc. Q cc/sec. Eq. (11)	Obs. Q	% error
1	31.47	18.07	29.0		8.64*	8.61	+ 0.4
2	28.57	18.07	29.0	6.40	7.72	6.61	+16.6
3	23.67	18.07	29.0	3.06	3.76	3.90	− 3.6
4	15.37	0.17	29.0	3.09	4.98	4.95	+ 0.6
5	14.37	0.17	29.0	2.70	4.47	4.55	− 1.8
6	9.57	0.17	29.0	1.18	2.37	2.50	− 5.2

* Calculated by Eq. (7)—composite flow, $Z_0 = 31.47$ cm, and showing the value of k to be accurate.

The capillary layer in run No. 2 was far from complete as will be noted, Z_1 being practically at sand height, $Z_s = 29$ cm. In this case the simple gravity formula gives a result only 3 percent low. The run is included here in order to show that the approximate correction may be made only in the case of a fairly complete capillary zone. No attempt has been made to handle the case of an incomplete zone. These data are intended to show the necessity of precaution in tests where appreciable capillary flow exists rather than to present a proof that Eq. (11) is accurate although it would appear that it is a fair approximation.

VI. Some Theoretical Considerations

Strictly speaking the problem of gravity flow may be considered as a potential problem for the determination of the velocity potential

$$\Phi = k(p + \gamma gz), \tag{12}$$

satisfying Laplace's equation

$$\partial^2\Phi/\partial x^2 + \partial^2\Phi/\partial y^2 + \partial^2\Phi/\partial z^2 = 0 \tag{12a}$$

and certain boundary conditions. These are: Φ = constant at outside boundary, Φ = constant at well surface. $-\partial\Phi/\partial z$ = vertical velocity = 0 at $z = 0$, $\Phi = k(p_0 + \gamma g z)$; $\partial\Phi/\partial n = 0$, at the free surface whose normal is n and which is at the uniform pressure p_0.

From this point of view the whole problem could be solved analytically by potential theory methods and the extended experimental investigation of the previous sections would be quite unnecessary. On the other hand, if we look at the boundary conditions, it seems that the problem is over-determined since we specify both Φ and its normal derivative at the free surface. And this discloses the fundamental difficulty of the problem which is that the free surface must be determined *simultaneously with* Φ and in such a way that the last of the above boundary conditions are satisfied. The solution to this problem would evidently involve an integral equation of considerable complexity, although in two-dimensional cases the methods of conjugate functions could be applied, as has been done so elegantly by Hopf and Trefftz (reference 3).

To get a quantitative description of the problem of gravity flow it was therefore necessary to make the empirical investigation and analysis described in the previous sections. Nevertheless it is of interest to see what some simple assumptions as to the nature of the flow will give in the form of a qualitative description of the problem. We consider first the velocities at the free surface.

Thus from the fact that Φ is a velocity potential it follows that the velocity V_s along the direction indicated by s which corresponds to the streamline $h(s)$ is:

$$V_s = -k(\partial p/\partial s + \gamma g \partial h/\partial s). \tag{13}$$

Since for the streamline defining the free surface, p is uniform, the velocity along the free surface is:

$$V_s = -k\gamma g \partial h/\partial s. \tag{13a}$$

The radial component is evidently:

$$V_r = -(k\gamma g dh/dr)/[1 + (dh/dr)^2]. \tag{13b}$$

To get further we shall assume that the fluid moves towards the well in cylindrical shells so that the radial velocity in the interior of the sand is independent of the vertical coordinates and hence is equal to that at the free surface. It follows then that the total flux, Q, through the sand is given by:

$$Q = -2\pi r V_r h(r) = +\frac{2\pi r k\gamma g(dh/dr)\, h(r)}{1 + (dh/dr)^2}. \tag{14}$$

Taking Q as known, Eq. (14) leads to the following differential equation for the free surface $h = h(r)$:

$$(dh/dr)^2 - (2\pi k\gamma g r h/Q)\, dh/dr + 1 = 0. \tag{15}$$

Since this equation, too, being nonlinear, is difficult to solve explicitly we make the further assumption that the slope of the free surface, dh/dr, is small so that its square may be neglected. We then get:

$$(2\pi k\gamma g r h/Q)\, dh/dr - 1 = 0 \tag{16}$$

with the integral:

$$h^2 - h_1^2 = (Q/\pi k\gamma g) \log r/r_1. \tag{17}$$[9]

This equation is evidently identical with that established empirically in §4 except that here the h refers to the actual height of the free surface whereas empirically Eq. (17) will be correct if h refers to the fluid head as measured at the bottom of the sand. This relation, however, must be considered as a fortunate coincidence since a little inspection will show that the two assumptions made in deriving Eq. (17) are definitely untenable and it is indeed surprising that the errors of these assumptions can be completely compensated by the simple change in the interpretation of h.

Thus, since

$$\partial V_r/\partial z = \partial V_z/\partial r$$

our assumption of shell flow ($\partial V_r/\partial z = 0$) implies that the vertical velocity, V_z, is independent of r and hence must vanish since it vanishes at the external boundary. But without vertical velocities the free surface would be horizontal and the flow would have no gravity characteristics. Further, it is not difficult to show that not only will V_r actually decrease as we approach the free surface, but even the total resultant velocity must decrease with increasing z.

That our neglect of $(dh/dr)^2$ in passing from Eqs. (15) to (16) is not strictly justified is still more obvious. For certainly near the well where the slope of the free surface approaches unity the first and last terms in Eq. (15) are of the same order of magnitude. The above derivation, which is equivalent to those in the literature except that it shows more clearly the nature of the assumptions made, can therefore be given no significance except as the present experimental study has established its *form* with regard to the pressure distribution at the bottom of the sand.

Nevertheless we can draw the following general conclusions from the above derivation. Thus, solving Eq. (13b), which is rigorously correct, for dh/dr we find

$$\frac{dh}{dr} = -\frac{k\gamma g}{2V_r} - \frac{1}{2}\left(\frac{k^2\gamma^2 g^2}{V_r^2} - 4\right)^{1/2}. \tag{18}$$

The plus sign before the radical would evidently correspond to a slope decreasing with V_r increasing. Since V_r is negative (it decreases with increasing r) it follows at once that the maximum value of dh/dr is 1, or that the maximum inclination that the free surface can have is 45°. When the inclination is 45° the radial velocity has its maximum

$$|\, V_{r_{\max.}} \,| = k\gamma g/2. \tag{18a}$$

[9] This is essentially the derivation given by others. Handbuch der Physik. **VII,** 117, except that heretofore the assumption of shell flow and neglect of $(dh/dr)^2$ have always been made at the beginning.

It follows still more generally from Eq. (13a) that since the horizontal velocity component at the free surface of *any* gravity flow system is:

$$V_h = -(k\gamma g \sin 2\theta)/2$$

where θ is the inclination of the free surface to the horizontal, the *maximum inclination of the free surface in any gravity flow system is 45°* and the maximum horizontal velocity component at the free surface is $k\gamma g/2$, which is half of the maximum vertical *free-fall* velocity. This does not imply that the free surface inclination increases uniformly until a value of 45° is reached, since in the actual radial flow case due to the change in medium at the well boundary, the free surface cuts the well face horizontally giving an inflexion at some distance from the well. Rather, the above results refer merely to the impossibility of obtaining inclinations exceeding 45° at *any* point of a gravity flow system.

As to the slopes of the stream lines below the free surface the following remarks may be made. Since the slope at any point is given by:

$$m = V_z/V_r$$

we have:

$$\partial m/\partial z = (1/V_r)[\partial V_z/\partial z - m(\partial V_r/\partial z)].$$

We have already seen that the radial velocity V_r, decreases as the free surface is approached, so that $\partial V_r/\partial z < 0$, considering the absolute values of the velocity components. Hence at such radii where the vertical velocities are increasing with the height the streamline slopes will increase as the free surface is approached and since the slope of the free surface cannot exceed 1, then neither will the streamlines have slopes exceeding 1. However, in the region near the well where the free surface undergoes an inflexion and its slope begins to decrease again the vertical velocity will also decrease so that for streamlines not far from the free surface it may well be that[10] $\partial V_z/\partial z < 0$ and finally that $\partial m/\partial z < 0$. Under such conditions it is possible that near the well the streamlines not much below the free surface may have slopes exceeding 1. This does correspond to the observations described in §3 although it should be mentioned that the capillary layer would produce a similar effect and may also be effective in causing the sharp slopes of the streamlines as observed in the experimental study.

VII. Generalizations and Conclusions

The above experiments and discussion have referred to the problem of gravity flow in a radial system. Although in practical cases where a well of small radius is draining its surrounding sand, the assumption of radial flow must represent a close approximation to the actual flow system up to appreciable distances from the well center, it is of some importance to be able not only to test this assumption but even to be able to treat gravity flow problems that definitely are not of the simple radial type. We shall therefore now

[10] This will in fact be necessary very near the well for small fluid heights in the well since then $\overline{V} \sim k\gamma g$ and since $V_z = 0$ at $z = 0$ and small at the free surface it must be appreciably larger and even approach $k\gamma g$ as one recedes from the free surface and enters the sand body.

present a generalization of the above results which is felt to be the natural extension of our point of view as to the significance of the Eqs. (7) and (8) established empirically.

Again as in the case of the radial flow problem, our generalization will not be new in its analytical *form*. For as long ago as 1886 Ph. Forchheimer[2] presented the equation:

$$\partial^2 Z^2/\partial x^2 + \partial^2 Z^2/\partial y^2 = 0$$

as governing the general case of gravity flow problems. Here again, however, the Z's are taken to refer to the *fluid heights* in the sand and the derivation of the equation is explicitly based on the assumptions of shell flow and the neglect of vertical velocities. These we have already seen to be physically unjustified as a region of fluid convergence is approached, and only fortuitously have they led in the case of radial flow to an analytical *form* empirically verified. Further, the computation of the flux at the well boundary would be totally in error if the above assumptions were logically applied since the actual discontinuity at the well face would give too large an area of outflow for the radial velocity computed by the above equation.

We therefore propose to consider the problem from the following point of view. We observe only that the result of the empirical study on the radial flow system, which is:

$$Z^2 = \frac{Z_1^2 - Z_2^2}{\log (r_1/r_2)} \log \frac{r}{r_1} + Z_1^2 \tag{19}$$

satisfies the equation:

$$\partial^2 Z^2/\partial x^2 + \partial^2 Z^2/\partial y^2 = 0 \tag{20}$$

with the boundary conditions:

$$\begin{aligned} Z &= Z_1 : r = r_1 \\ Z &= Z_2 : r = r_2 \end{aligned} \tag{21a}$$

where Z refers only to the fluid pressure head at the bottom of the sand. Since even a radial flow system corresponds to some degree of geometrical complexity we now generalize and postulate that Eq. (19) holds for *every* gravity flow system with a horizontal impermeable base with arbitrary boundary conditions.

To get the total flux Q through a general gravity flow system we proceed as follows. Since at the high fluid level boundary the free surface slopes are necessarily small and the height of the free liquid surface actually coincides with the boundary value of the pressure head Z, we are justified in using the assumption of shell flow *at this boundary* and to identify the fluid height with the fluid head. We have then by D'Arcy's law:

$$Q = k\gamma g \int Z \frac{\partial Z}{\partial n}\, ds = \frac{k\gamma g}{2} \int \frac{\partial Z^2}{\partial n}\, ds \tag{21}$$

where : k, γ, g have the same meaning as usual, n is the external normal at the element ds of the boundary curve of the region, and the integral is extended about the whole of this boundary curve. Thus for the case of radial flow we have by Eq. (19):

$$Q = \frac{k\gamma g}{2} \int \frac{Z_1^2 - Z_2^2}{\log(r_1/r_2)} \frac{1}{r} (r d\theta) = \frac{\pi k\gamma g(Z_1^2 - Z_2^2)}{\log(r_1/r_2)}$$

which is identical with that given by Eq. (4) and verified empirically.

For linear flow in a sand column of length L the solution to Eq. (20) would evidently be:

$$Z^2 = (Z_1^2 - Z_2^2)x/L + Z_2^2$$

so that

$$Q = \frac{k\gamma g}{2} \int \frac{Z_1^2 - Z_2^2}{L} ds = \frac{k\gamma g}{2} \frac{Z_1^2 - Z_2^2}{L} s \tag{22}$$

where s is the width of the linear flow section. Eq. (22) has also been verified experimentally by measurements on a linear flow tank in a manner exactly the same as used for the radial flow experiments. This may be considered at least as a partial justification for the generalization of Eq. (20) for other than radial flow systems.

If at the high fluid level boundary the liquid extends above the sand thickness we again have a composite flow case. The treatment then will follow exactly the lines of §5. Thus the gravity fluid heads Z_g will be obtained by the solution of Eq. (21) with boundary conditions:

$$Z_g = Z_2 \text{ at boundary (2)},$$
$$Z_g = Z_s \text{ at boundary (1)};$$

where Z_s is the sand thickness; then the nongravity component Z_n is to be found as usual from the equation

$$\partial^2 Z_n/\partial x^2 + \partial^2 Z_n/\partial y^2 = 0 \tag{23}$$

with the boundary conditions

$$\begin{aligned} Z_n &= Z_s \text{ at boundary (2)}, \\ Z_n &= Z_1 \text{ at boundary (1)}, \end{aligned} \tag{23a}$$

where Z_1 and Z_2 are the actual fluid heads at the boundaries (1) and (2) respectively it being assumed, of course, that

$$Z_1 > Z_s > Z_2.$$

The resultant fluid head distribution will then be:

$$Z = Z_g + Z_n - Z_s.$$

Similarly the resultant flow through the system will be given by:

$$Q = k\gamma g \int (Z\partial Z/\partial n)_s ds = k\gamma g Z_s \int (\partial Z/\partial n) ds$$

$$= (k\gamma g/2) \int (\partial Z_w^2/\partial n) ds + k\gamma g Z_s \int (\partial Z_n/\partial n) ds.$$

These equations will suffice to determine everything of interest about any gravity flow problem in a homogeneous sand with a horizontal impermeable bottom boundary, with the exception of actual fluid heights in the sand throughout the system. In practical cases the effects of capillarity, which are not included in the above expressions for Q will be of negligible importance.

The authors wish to acknowledge the assistance of Dr. H. T. Kennedy in some of the earlier experimental work on this problem.

A Theory of Surface Conductance at an Electrolyte-Solid Interface

By KENNETH S. COLE[1]
Department of Physiology, Columbia University

(Received June 7, 1932)

An expression has been derived on the basis of the Maxwell-Boltzmann distribution and Poisson's equation for the tangential surface conductance of an electrolyte in contact with a charged plane surface. One part of this expression is analogous to the result given by Smoluchowski for a Helmholtz double layer, while the second part arises from the movement of the ions in the diffuse ion cloud under the applied electric field. The theory shows qualitative agreement with the data of Briggs for the conductance of univalent chloride solutions at a cellulose surface. For all but the most dilute solutions, the Smoluchowski term is negligible and the surface conductance is proportional to the charge density on the surface. The theory does not agree with the data for different anions and it is suggested that the discrepancy may be due to absorption phenomena. There may be a movement of the adsorbed ions or of a diffuse ion cloud resulting from the presence of adsorption potentials at a distance from the interface.

ASSUMING the presence of a Helmholtz double layer at the surface of a solid in contact with an electrolyte, Smoluchowski, (1905), showed that there should be a surface conductivity due to the movement of the layer of charge in the electrolyte, when an electric field is applied parallel to the interface. Such conductivities have been reported by Stock (1912), McBain (1921, 1929), Fairbrother and Mastin (1924), Stamm (1926), Briggs (1928), and Gortner (1931, 1932), and his associates. It is now well known that the Helmholtz concept of a rigid double layer may be replaced by a diffuse ion cloud in which the concentration of ions in the neighborhood of a charged surface is given by the Maxwell-Boltzmann principle and the Coulomb forces, cf. Gouy (1910), Chapman (1913), Hertzfeld (1920), Gyemant (1923), Stern (1924).

Following Debye and Hückel (1923), it will be assumed that we are dealing with a dilute solution of a strong electrolyte in which the average concentration of the i ion is $\bar{n}_i$ and its valence is z_i. Then, where the electric potential is ψ, the concentration of the i ion n_i is given by the Maxewll-Boltzmann distibution function,

$$n_i = \bar{n}_i e^{-z_i \epsilon \psi / kT} \doteq \bar{n}_i (1 - z_i \epsilon \psi / kT), \tag{1}$$

where ϵ is the electronic charge, k is the Boltzmann constant and T is the absolute temperature. The free charge density is then

$$\rho = \sum n_i z_i \epsilon = -(\epsilon^2 \psi / kT) \sum \bar{n}_i z_i^2.$$

Substituting in the Poisson equation

$$\text{div grad } \psi = -\frac{4\pi\rho}{D} = \frac{4\pi\epsilon^2\psi}{DkT} \sum \bar{n}_i z_i^2 = \kappa^2 \psi;$$

[1] The major portion of this work was done as an International Education Board Fellow at the Physikalisches Institut, Universität Leipzig in 1928–29.

where

$$\kappa^2 = (4\pi\epsilon^2/DkT) \sum \bar{n}_i z_i^2.$$

For the semi-infinite one dimensional case with a plane at $y=0$,

$$d^2\psi/dy^2 = \kappa^2\psi \quad \text{and} \quad \psi = Ae^{-\kappa y} + Be^{\kappa y}.$$

Since ψ must remain bounded, $B=0$. When the surface charge density is σ

$$(d\psi/dy)_{y=0} = -A\kappa = -4\pi\sigma/D$$

and

$$\psi = (4\pi\sigma/D\kappa)e^{-\kappa y}. \tag{2}$$

By substituting in (1)

$$n_i = \bar{n}_i\left(1 - \frac{\sigma}{\kappa}\cdot\frac{4\pi z_i\epsilon}{DkT}e^{-\kappa y}\right) = \bar{n}_i\left(1 - \frac{\Delta n_i}{\bar{n}_i}\right),$$

where

$$\Delta n_i = \bar{n}_i - n_i.$$

If an electric field E is applied parallel to the plane, then because of the net charge density resulting from the unequal concentrations of the ions of opposite sign there is a body force on the liquid,

$$F = E\rho = (-ED/4\pi)\cdot(d^2\psi/dy^2).$$

When the viscosity of the liquid is η, for one dimensional laminar flow, the velocity u_s is given by

$$F + \eta d^2u_s/dy^2 = 0$$

and

$$-\frac{ED}{4\pi}\cdot\frac{d^2\psi}{dy^2} + \eta\frac{d^2u_s}{dy^2} = 0.$$

Integrating,

$$u_s = (ED/4\pi\eta)(\psi - \psi_0)$$

since $u_s = 0$ when $\psi = \psi_o$ and $y=0$. Then from Eq. (2) we have

$$u_s = -(E\sigma/\eta\kappa)(1 - e^{-\kappa y})$$

which is the motion of the liquid due to the body force.

Since this body force is the result of the viscous drag of the ions on the liquid we must also consider the velocity of the ions relative to the medium,

$$u_i = Ez_i/\rho_i$$

where ρ_i is the friction coefficient of the i ion, so the total velocity of the ion relative to the plane is

$$u_i' = u_s + u_i.$$

The current density

$$J = \sum u_i' n_i z_i\epsilon = \sum(u_s + u_i)\left(1 - \frac{\Delta n_i}{\bar{n}_i}\right)\bar{n}_i z_i\epsilon$$

$$= \sum u_s\bar{n}_i z_i\epsilon - \sum u_s\Delta n_i z_i\epsilon$$

$$+ \sum u_i\bar{n}_i z_i\epsilon - \sum u_i\Delta n_i z_i\epsilon.$$

Subtracting the current density due to the bulk conductance λ of the electrolyte we have $\Sigma \bar{n}_i z_i \epsilon = 0$ and $\Sigma \bar{n}_i z_i \epsilon u_i = \lambda$ and the surface conductance current density is

$$\Delta J = J - E\lambda = \frac{E\sigma}{\eta\kappa} \cdot \sigma\eta(1 - e^{-\kappa y}) - \frac{E\sigma}{\kappa} \cdot \frac{4\pi\epsilon^3}{DkT} e^{-\kappa y} \sum \frac{\bar{n}_i z_i^3}{\rho_i} .$$

The surface conductance for a unit square of surface is then

$$\Delta\lambda = \int_0^\infty \frac{\Delta J}{E}\, dy = \frac{\sigma^2}{2\kappa\eta} - \sigma\epsilon \frac{\sum \bar{n}_i z_i^3/\rho_i}{\sum \bar{n}_i z_i^2} . \tag{3}$$

The first term is the counterpart of Smoluchowski's result and is due to the net charge carried by the motion of the solvent while the second term, due to the motion of the ions through the solvent, apparently has not been considered except by Mooney (1931).

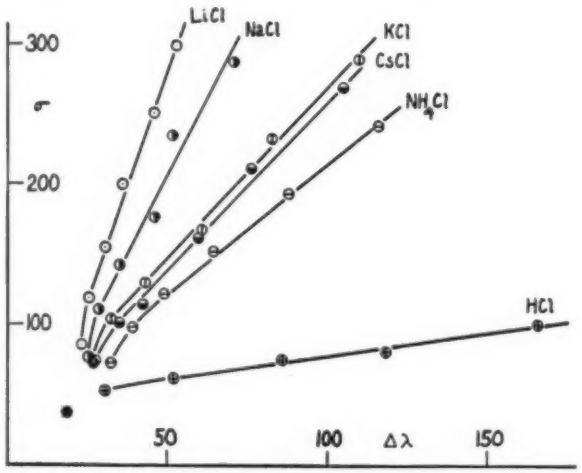

Fig. 1. $\Delta\lambda$, the surface conductivity in reciprocal megohms *vs.* σ, the surface charge density in e.s.u./cm^2, from data of Briggs on cellulose.

Since either σ or ψ_0 must be known, the only data available with which to test Eq. (3) are for the surface conductance of packed cellulose fibers—of which those of Briggs (1928) are representative. These data for the univalent chlorides have been corrected for the ionic strength of the distilled water by Abramson (1932), who showed that there is a general parallel between σ^2/κ and $\Delta\lambda$ as predicted by Smoluchowski. It is found, however, that this term becomes smaller with increasing salt concentration since κ increases faster than σ^2 and that for a uni-univalent salt in which the mobilities of the two ions are quite different, the second or mobility term is considerably more important. On the assumption that for all except the lowest concentrations the Smoluchowski term would be negligible, σ has been plotted against $\Delta\lambda$ in Fig. 1. The linear relationships at the higher concentrations are quite striking in their qualitative agreement with the theory. It is unfortunate that it is not possible to make an accurate check on the correctness of the magnitude of the specific surface conductance as given by the theory because of the

complex nature of the surfaces in such a diaphragm of packed cellulose fibers. An approximate calculation based on an assumed cell length of 1 cm gave the sum of the perimeters of the transverse sections for all fibers of such a diaphragm as about 10^4 cm. This does not seem an impossible value. Assuming a reasonable value for ψ_0, Mooney (1931) calculated $\Delta\lambda$ for glass to be 0.02 of the conductance given by McBain (1929). Since White, Urban, and Van Atta (1932) extrapolate a value 0.03 of that of McBain's, they agree rather well with Mooney.

There is, however, a very marked disagreement between the theory and experiment. Since the mobility term is proportional to the differences of the mobilities of the two ions, it should not contribute to the surface conductance of KCl. This is most decidedly not the case,—in fact the effect of Cl^- seems too large for all of the salts. The approximation involved in the expansion of the exponential in Eq. (1) is not serious enough to explain the discrepancy when the maximum value of ψ_0 is 13 mv. The interionic forces in the electrolyte and their modification in an electric field have not been considered. These effects should be treated by the methods of Onsager (1927) and Debye and Falkenhagen (1928), but Wagner (1924) showed the former effect to be negligible for the negative adsorption at an air-electrolyte interface. The assumption of a semi-infinite electrolyte at a plane interface may be replaced by one of a tube of electrolyte bounded by a cylindrical interface. If the radius γ_0 of this tube is small so that $\kappa\gamma_0 < < 1$, the approximations to the Bessel's functions of the solution lead to the result that ψ_0, σ and $\Delta\lambda$ are independent of κ. This is not in agreement with the data.

By comparison of the surface conductances of the various electrolytes, at a given surface charge density, with the ionic mobilities, it is found that the effect of the Cl^- ion is fairly constant and considerably more important than is indicated by Eq. (3). This suggests that either the adsorbed charge or the adsorption forces may play a role in these phenomena. If the adsorption forces are not effective at distances greater than molecular or ionic dimensions, then there is the possibility of a net motion of the adsorbed ions under the influence of a tangential electric field as well as a two dimensional Brownian movement, cf. McBain and Salmon (1921), Volmer (1922). In this case, the surface conductance due to the adsorbed ions would be

$$\Delta\lambda' = \sum \frac{n_i z_i^2 \epsilon^2}{\underline{\rho_i}}$$

where $\underline{n_i}$ and $\underline{\rho_i}$ are the "*concentration*" and "*mobility*" of the ion on the surface. This hypothesis will explain quite well the experimental observations for uni-univalent electrolytes, where the form of the σ *vs.* concentration curve suggests a preponderate adsorption of the negative ion, cf. Abramson and Müller (1932). It is also in agreement with the observation of Briggs (1928) that $\Delta\lambda \neq 0$ when $\psi_0 = 0$ for certain polyvalent electrolytes. If ions of both signs are adsorbed such that for some concentration $\sigma = 0$, both the Smoluchowski and the mobility conductances will vanish, while this adsorption conductance is not necessarily zero. Langmuir (1918), Gyemant (1923),

Stern (1924) and Hückel (1928) have assumed that the sphere of action of adsorption forces is of the order of molecular dimensions, but according to Trillat (1926) it can be shown that for liquids at an unsaturated interface these forces may be effective at a considerably greater distance. The corresponding adsorption potential would cause the formation of a diffuse ion cloud near the interface in much the same manner as the electric potential considered above. This adsorption ion cloud would then give rise to an added surface conductance without the assumption of mobility of ions adsorbed at the interface. The analysis of this case by the Maxwell-Boltzmann distribution would require for adsorption potentials the counterpart of Poisson's equation in electrostatics—since the inverse square law of force action would not be expected to be immediately applicable.

In conclusion it might be pointed out that such adsorption factors as these considered may play an important part in other electrokinetic phenomena and that careful experiments of the type performed by Briggs but of a more absolute character are greatly to be desired.

I wish to express my thanks to Professor P. Debye and to Dr. H. A. Abramson for their interest and assistance in this problem.

References

H. A. Abramson, J. Phys. Chem. (in press).
H. A. Abramson and H. Müller, Presented at New Haven meeting, American Physical Society, (1932).
D. R. Briggs, Colloid Symposium Mon. **6,** 41 (1928). J. Phys. Chem. **32,** 1646 (1928).
H. B. Bull and R. B. Gortner, Colloid Symposium Ann. (New York) **8,** 309 (1931). Physics **2,** 21 (1932).
D. L. Chapman, Phil. Mag. **25,** 475 (1913).
P. Debye and H. Falkenhagen, Phys. Zeits. **29,** 401 (1928).
P. Debye and E. Hückel, Phys. Zeits. **24,** 185 and 334 (1923).
Fairbrother and Mastin, J. Chem. Soc. **125,** 2319 (1924).
A. Gouy, Jour. de Physique (4), **9,** 457 (1910).
A. Gyemant, Zeits. f. Physik **17,** 190 (1923).
K. F. Herzfeld, Phys. Zeits. **21,** 28 (1920).
E. Hückel, *Adsorption and Kapillarkondensation.* Leipzig, (1928).
I. Langmuir, J.A.C.S. **40,** 1361 (1928).
J. W. McBain, J.A.C.S. **51,** 3294 (1929).
J. W. McBain and Darke, Kolloid Z. **28,** 239 (1921).
J. W. McBain and Salmon, Proc. Roy. Soc. **A98,** 398 (1921).
M. Mooney, Colloid Symposium Ann., (New York) **8,** 331 (1931).
L. Onsager, Phys. Zeits. **28,** 277 (1927).
Stamm, Colloid Symposium Mon. (New York) **4,** 246 (1926).
O. Stern, Zeits. f. Elektrochem. **30,** 508 (1924).
J. Stock, Anz. Akad. Wiss. Kracov (A) 635 (1912).
M. v. Smoluchowski, Phys. Zeits. **6,** 529 (1905).
Trillat, Ann. de Physique **10,** 5 (1926).
Volmer, Zeits. f. physik. Chem. **102,** 267 (1922); Zeits. f. Physik **9,** 193 (1922).

THE EDITOR'S COLUMN

Interaction of Light and Sound Waves

IN A recent paper by Debye and Sears attention is directed[1] to a very pretty experiment on light scattering in liquids. Originally suggested by L. Brillouin[2] in 1922 from theoretical considerations, it has recently been carried out in connection with experiments made on the Raman effect in liquids.

It is a familiar fact that in a homogeneous medium the propagation of light takes place very much as it does in free space; i.e., in "straight lines" and with uniform velocity. (That the velocity of propagation is less than in free space is not of importance from this particular point of view.) On passing the boundary separating two such individually homogeneous regions the light is subject to a change, however, and generally speaking is partly transmitted (refracted) and partly reflected, so that the discontinuous variation in the optical properties at the boundary separating the two media leads to a "breaking up" of the light, to which the general term *scattering* can be applied.

Naturally, the transition boundary between two media is not really discontinuous, but can be thought of as a thin layer within which the properties of the one medium vary rapidly to those of the other. If we wish to treat the boundary as though it were perfectly sharp we can do so by considering it as the ideally limiting case of a very thin but finite transition layer.

Similarly, a medium whose properties vary in a continuous manner from point to point can be treated as the limiting case of a conglomerate of small homogeneous regions with discontinuous boundaries. As a physical illustration we recall the familiar fact that sand of which the individual particles are very minute has many of the properties of a liquid, for example, that of *flowing*. If one grinds the sand grains finer and finer into a powder the sand behaves more and more like a liquid. What we wish to see from this for our present purpose is that in traversing such a conglomerate of minute particles (such as a "sand" made of glass particles) light would be refracted and reflected at each one of the boundaries between particles, so that it would be gradually dispersed or "scattered." Even in the limiting case in which the sizes of the particles become infinitesimal this scattering effect persists, even though the medium can be finally treated as being continuous (but of course not uniform).

The upshot of the matter is that inhomogeneities in a substance traversed by light, will lead to a scattering of the light. It is immaterial how the inhomogeneities are produced, whether by mechanical stresses, nonuniform heating or in any other way. We may recall in passing the extensive use which is being made of this fact in the testing of stresses in bridges and the like by constructing glass models through which light is passed. The inhomogeneities produced by the strains in the glass produce visible colorations which can be readily studied.

The basic idea of the experiments treated by Debye and Sears is that if an otherwise optically transparent medium is transmitting sound waves then the fluctuations of pressure within the sound wave will produce inhomogeneities in the density of the transmitting medium of just the type which we have been discussing, so that if light is passed through the medium it should be scattered. We are thus justified in speaking of an *interaction* of light and sound, or of a scattering of light by sound. These terms hardly do the phenomenon justice but at least they give succinct expression to it.

This idea of Brillouin's opens up a number of suggestive lines of thought. For example, if we consider the simplest case of a *plane* sound wave of wave-length l, then the distance between a region of maximum pressure and one of minimum pressure in the wave is $l/2$, and

[1] P. Debye and F. W. Sears, Proc. Nat. Acad. Sci. **18,** 409 (1932). See also E. H. L. Mayer and W. Ramm, Phys. Zeits. **33,** 270 (1932).

[2] L. Brillouin, Ann. de Physique **17,** 88 (1922).

since these regions are separated in space by regular intervals, they present an array similar to a *grating*. Can one then expect to find an action on the light similar to the action of a grating? Will one find interference phenomena associated with fluctuations in intensity of the light "reflected" from this grating?

The answer given by theory is in the affirmative, and this has been verified by the experiments. In the arrangement of Debye and Sears the "sound waves" were generated artificially in a liquid by immersing a piezoelectric crystal in it. On setting the crystal into oscillation its motion was transmitted to the liquid. The liquid was contained in a vessel with transparent walls through which light could easily be transmitted, and the scattered light examined as it emerged from the other side. The light scattered at different angles with the direction of the primary beam was examined in order to look for the interference patterns of which we have spoken, and which are due to the grating character of the sound waves. These patterns were readily found.

It is of particular interest to note that all of the scattered light does not have the same wave-length as the incident light. This is due to the fact that the sound waves in the liquid are *travelling* and not *standing* waves. If we use the simplified idea of the scattering process as being simply a reflection of the light from a set of moving parallel planes (or mirrors) then we must expect that there will be a Doppler effect giving rise to scattered light of frequency $\nu[1 \pm 2(v/v') \sin(\theta/2)]$ where ν_0 is the frequency of the incident light, v' the velocity of the light *in* the liquid, v the velocity of the sound waves in the liquid and θ the angle between the directions of the incident and scattered light. Since there is always some scattering due to dust particles, motes, and the like in the liquid, (and also some scattering due to the Raman effect of individual molecules) without change of frequency of the light, one must expect to find light of three frequencies in the scattered radiation, and of course if one could measure the change in frequency of the scattered radiation accurately a determination of v, the velocity of sound in the liquid, could be made. This has been verified experimentally and preliminary measurements of this nature are reported by Debye and Sears.

Actually the experimental results are somewhat more complicated and require a more detailed theory than we have been able to give here, principally due to the finite size of the actual apparatus which precluded the possibility of setting up purely harmonic plane waves in the liquid. The authors state that the scattered light can easily be made of sufficient intensity for projection on a screen, which of course cannot be done with the feeble scattered radiation in the Raman effect, and which would serve to give an audience a vivid picture of the process of light scattering.

E. L. HILL

Quantum Mechanics and Optics

THROUGHOUT the whole period of development of quantum mechanics considerable interest has attached to the analogy with optics and Newtonian mechanics, an analogy which can be roughly stated in the form of a proportion:—

Quantum mechanics: Newtonian mechanics:: Physical optics: Geometrical optics.

The proportion is of course imperfect, but is indicative of the formal analogy. The relationship between geometrical optics and Newtonian mechanics was discovered years ago by the eminent geometrician and logician, Sir William Rowan Hamilton, but the complementary relationship between quantum mechanics and physical optics was not discovered until about 1924 when L. de Broglie developed his ideas on the wave nature of matter. The latest link in this chain of reasoning is furnished in a paper by W. Pauli[1] who has analyzed the relationship existing between the relativistic wave equation of Dirac and the dynamics of the special theory of relativity.

During the early period of development of quantum mechanics there was a great deal of discussion concerning the role played by the Planck constant h. It was observed to be a general rule that whenever a formula found by means of quantum theory did not contain h, then that formula could be (and in most cases already had been) developed directly from classical electron theory: and if, on the other hand, h appeared explicitly in the formula then the classical theories gave either bad answers or else no answers at all to the

problem. This made it seem pretty certain that there must be a close relation between the equations of the "true" quantum theory and those of the classical theory, associated in some manner with the limit $h \to 0$. So far as the nonrelativistic wave equation of Schrödinger is concerned, the method for making this comparison was developed independently by G. Wentzel and L. Brillouin.

Before delving into this problem let us examine some of the physical elements of the problem. In the Newtonian dynamics, say for a single particle, one proposes to obtain equations stating the coordinates of the particle as a function of time; i.e., $x(t)$, $y(t)$, $z(t)$. The method for doing this is to solve the differential equations for the motion, assuming that the analytical expressions for the components of the force are known; to complete the solution one must specify the way in which the particle is started off, that is, its initial position and velocity. When all of these things have been stated the solution of the equations of motion will give one the path or trajectory followed by the particle, and they will give in addition all information concerning the way in which the particle traverses this path—its velocity at any point, its time of arrival at any point, etc. In other words, we get a complete time table for the touring particle. This beautifully simple idea of a point travelling along a definite curve in a perfectly definite manner can easily be extended to more complex systems by considering the motion of a single "representative" point in a (mathematical) space having as many dimensions as the system has degrees of freedom.

But instead of thinking of a single particle being started off from a given point at some definite instant we can think of a very large number of particles all having the same total energy but being started off from a variety of points. The particles are all supposed to move in the same "external" field of force without influencing each other. We shall then have the picture of a swarm of "touring" particles all travelling along their individual paths. Since the potential energy of a particle may be considered as a definite function of position, the speed of the particles depends only on the particles' positions (and of course on its total energy which is the same for all particles by hypothesis).

The analogy with geometrical optics can now be made by the following observation, the proof of which is given by the Hamilton-Jacobi dynamical theory. Suppose we set up in the field of force a surface, the form of which is arbitrary (but which for simplicity we may visualize as a portion of a sphere). Let us consider a swarm of particles all starting at the same instant from different points on the surface with the velocities appropriate to those points and travelling away from the surface in the same direction. The paths of these particles will then form a family of curves orthogonal to the given surface. If we now imagine the family of surfaces orthogonal to this family of curves (and of which the original surface is one member) drawn in, then the proof referred to shows that all of the particles move together in such a way that at any instant they all lie together on a single member of this family of surfaces. Or, if we imagine a surface drawn at every instant in such a way that the set of particles all lie in it, then this surface, as it travels along with the particles, continuously adjusts itself so that it "fits" some member of the family of surfaces. The analogy with geometrical optics is now clear—the family of surfaces are the analogs of the *surfaces of constant phase* for the light, while the paths of the particles; i.e., the orthogonal trajectories to the surfaces are the analogs of the *rays* of the light. If at this point one takes the trouble to adjust the equations of motion of the particles, in particular the force equation, then it is possible to develop a quite sensible theory of photons to replace the mass particles with which we commenced. In this way *geometrical* optics, combined with dynamical theory leads at once to a corpuscular theory of light.

This is all very well, but we know that geometrical optics fails to give any description of such important phenomena as scattering, diffraction, dispersion, etc. Just so does Newtonian dynamics fail to give an account of the analogous phenomena for *matter* waves as we now understand them; and just as there is no bridge for the gap between Fermat's theorem which lies at the basis of geometrical optics and the optical wave equation which forms the foundation of physical optics, so there is no bridge for the gap between Newton's equations of motion and Schrödinger's equation. There is the analogy, and fortunately this has been sufficient to give us a start.

We know that the differences between the predictions of physical and geometrical optics

become ironed out in the case of light with small wave-length. Practically, of course, this takes us into the regions of x- and γ-rays when neither theory really applies, but formally the two sets of *equations* merge into each other if we take the limit $\lambda \to 0$, where λ is the wave-length of the light. If we look for an analogous degeneration of quantum mechanics into Newtonian mechanics we find it in precisely the same way when we take as the wave-length of a mass particle the de Broglie expression $\lambda = h/mv$, m being the mass of the particle, v its velocity, and h Planck's constant.

But now we see the meaning which is to be attached to the formal limit $h \to 0$ which we spoke of at the beginning of this note, and which seems a little awkward since h is a perfectly definite and finite quantity! The answer is that the proper "physical" limit is not $h \to 0$, but $\lambda \to 0$ which can be approached by considering $m \to \infty$ or better $v \to \infty$. For high-velocity particles then, those distinguishing features which separate the quantum mechanical description of their behavior from that of Newton's dynamics disappear.

The only fly in the ointment now is that it is known that for high-velocity particles one should replace the Newtonian dynamics again by the dynamics appertaining to at least the special theory of relativity. And as for the wave equation of Schrödinger, we guess that Dirac's relativistic equation is the proper first substitute.

The partial justification that this procedure is in the right direction constitutes one of the most interesting points in Pauli's paper,[1] in that he actually carries through the demonstration that the dynamical equations of relativity theory are the zeroth order approximation to Dirac's equation. The demonstration proceeds along the lines of the previous treatment of Wentzel and Brillouin which we have already mentioned, and which in essence is an expansion of the solution of the quantum-theory equations as a series in powers of h (although not in a simple Taylor's or power series).

In the first approximation involving h, which is that in which deviations from the "geometrical optical" properties of the relativistic dynamics become apparent, Pauli finds that the peculiar effects due to the *spin* of the electron also appear. By studying the behavior of the electron in a one-dimensional field of force he has been able also to study more carefully the so-called *Klein Paradox* according to which a mass particle can change the *sign* of its mass, an electron thus behaving effectively like a proton of mass 10^{-27} g, for the detailed consideration of which we must refer to the original article.

It is especially interesting to notice in these investigations how a small variation in the formal appearance of a set of equations can change so radically their properties and the associated physical interpretation.

E. L. Hill

[1] W. Pauli, Helvetica Physica Acta **5**, 179 (1932).